UC Davis
UC Davis Previously Published Works

Title
Roundness of grains in cellular microstructures

Permalink
https://escholarship.org/uc/item/9r80x5vw

Journal
Physical Review E, 96(2)

ISSN
2470-0045

Authors
Lutz, FH
Mason, JK
Lazar, EA
et al.

Publication Date
2017-08-01

DOI
10.1103/physreve.96.023001

Peer reviewed

Roundness of grains in cellular microstructures

F. H. Lutz*
Technische Universität Berlin, 10623 Berlin, DE.

J. K. Mason†
Boğaziçi University, Bebek, Istanbul 34342, TR.

E. A. Lazar‡
University of Pennsylvania, Philadelphia, PA 19104, USA.

R. D. MacPherson§
Institute for Advanced Study, Princeton, New Jersey 08540, USA.
(Dated: October 11, 2018)

Many physical systems are composed of polyhedral cells of varying sizes and shapes. These structures are simple in the sense that no more than three faces meet at an edge and no more than four edges meet at a vertex. This means that individual cells can usually be considered as simple, three-dimensional polyhedra. This paper is concerned with determining the distribution of combinatorial types of such polyhedral cells. We introduce the terms *fundamental* and *vertex-truncated* types and apply these concepts to the grain growth microstructure as a testing ground. For these microstructures we demonstrate that most grains are of particular fundamental types, whereas the frequency of vertex-truncated types decreases exponentially with the number of truncations. This can be explained by the evolutionary process through which grain growth structures are formed, and in which energetically unfavorable surfaces are quickly eliminated. Furthermore, we observe that these grain types are 'round' in a combinatorial sense: there are no 'short' separating cycles that partition the polyhedra into two parts of similar sizes. A particular microstructure derived from the Poisson–Voronoi initial condition is identified as containing an unusually large proportion of round grains. This Round microstructure has an average of 14.036 faces per grain, and is conjectured to be more resistant to topological change than the steady-state grain growth microstructure.

PACS numbers: 61.72.-y, 61.43.Bn, 05.10.-a

I. INTRODUCTION

Many physical and biological systems share the property of being composed of irregular polyhedra subject to some form of energy minimization. The microstructures of polycrystalline materials in general and of metals in particular [1, 2] often serve as motivating examples, and can be modeled as resulting from a process of three-dimensional grain growth subject to isotropic boundary energies and mobilities [3, 4]. A portion of the resulting simulated microstructure is given in Figure 1, with some isolated grains displayed in Figure 2.

An investigation of these figures reveals several significant features. First, the networks of edges on the surfaces of the grains are connected in many different ways (i.e., the number of topological types is large). While this could be explained as the result of some inherent disorder in a physical system that is constrained to be space-filling, the distribution of topological types has been observed to be far from random [5]. Still, relatively little

is currently known about why certain types appear more frequently than others. Second, the examples in Figure 2 show that many of the grains appear to be geometrically round, in the sense of the surface area to volume ratio. This could be explained as the result of energy minimization, since the energy of the model system is proportional to the sum of the surface areas of the grains. A reasonable question would be whether this property is related to the observed distribution of topological types (e.g., the topological types in a material with equiaxed grains are likely different from those in a material with extruded grains).
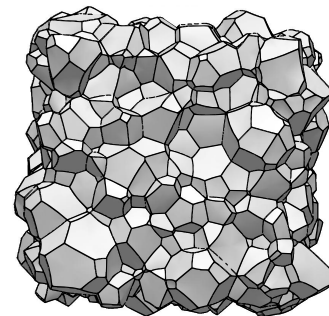

FIG. 1. A simulated microstructure resulting from a process of grain growth, assuming isotropic grain boundary energies and mobilities.

* lutz@math.tu-berlin.de
† jeremy.mason@boun.edu.tr
‡ mlazar@seas.upenn.edu
§ rdm@math.ias.edu

TABLE I. Glossary of terminology appearing throughout the article, listed alphabetically.

| Term	Description
1-skeleton	The restriction of a triangulation to the vertices and edges.
3-polytope	A three-dimensional convex solid with flat polygonal faces.
combinatorially k-round	A simple 3-polytope that is obtained from the tetrahedron or a flag* simple 3-polytope by at most k vertex truncations.
complete subgraph	A subgraph for which every pair of vertices is connected by an edge.
degenerate grain	A grain where one of the faces is a 2-gon or two faces share more than one edge.
dual graph	For a set of faces of a 3-polytope, the dual graph contains a vertex for every face in the set, and an edge connects vertices whenever the corresponding faces share an edge.
dual polytope	For a polytope P, the dual polytope P^* has faces and vertices in an incidence-preserving correspondence with the vertices and faces of P.
dual triangulation	For the boundary of a simple 3-polytope, the dual triangulation is the boundary of the dual polytope.
flag(*)	A flag* simple 3-polytope has no triangular faces or non-trivial 3-belts. A flag simplicial 3-polytope is dual to a flag* simple 3-polytope.
fundamental	A simple 3-polytope that is either the tetrahedron or does not have any triangular faces.
ℓ-belt	A set of ℓ faces of a simple 3-polytope such that the dual graph is a triangulated circle.
Schlegel diagram	A projection of the boundary of a 3-polytope onto one of its faces in such a way that vertices not belonging to the face lie inside it and no two edges cross.
severely constricted(*)	A severely constricted simple 3-polytope has no triangular faces but at least one non-trivial 3-belt. A severely constricted* simplicial 3-polytope is dual to a severely constricted simple 3-polytope.
simple	A 3-polytope where two faces meet on at most one edge and exactly three faces meet at each vertex.
simplicial	A 3-polytope where every face is a triangle. The boundary is a triangulation of the sphere S^2.
split type	A flag* simple 3-polytope has split type $k : \ell : m$ if k is the largest integer less than or equal to m such that the polytope has an ℓ-belt and the removal of this belt leaves two disks of k and m faces.
stacked(*)	A stacked* simple 3-polytope is obtained from the tetrahedron by a sequence of vertex truncations. A stacked simplicial 3-polytope is dual to a stacked* simple 3-polytope.
trivial 3-belt	A 3-belt where the three faces share a unique vertex.
vertex-truncated	A simple 3-polytope that is not the tetrahedron and has at least one triangular face.
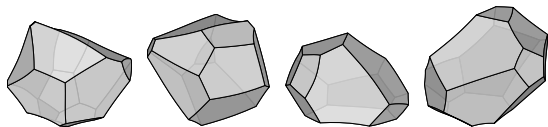
FIG. 2. A typical set of grains from the grain-growth microstructure.

The purpose of this paper is threefold. First, some language and concepts inspired by combinatorial topology are introduced to make the discussion and classification of the topological types of grains more precise, and to provide a framework to compare the distribution of topological types in different systems. These are intended to be generally useful for the analysis of cellular structures. Data from simulations suggest that the dynamics of grain growth in real space induce dynamics on the space of topological types, involving the switching of edges and the creation and deletion of triangular faces. The second purpose of the paper is to offer a preliminary description of these dynamics. Third, a detailed investigation of the evolution of a microstructure from a typical initial condition reveals a point where the grains appear to be particularly round in a specific combinatorial sense. This seems to result from triangular faces in the initial condition disappearing before triangular faces on tetrahedral grains can appear in comparable numbers. The possibility that this microstructure is particularly stable to thermal coarsening suggests a further investigation into the properties of the corresponding experimental microstructure.

II. COMBINATORIAL ANALYSIS OF CELLULAR MICROSTRUCTURES

A. Simple and Simplicial Polytopes

A *three-dimensional polytope* (3-polytope) is defined as a three-dimensional convex hull of finitely many points in three-dimensional space. With only a few degenerate exceptions (described in Section IV), most of the grains observed in the simulated grain growth microstructures (or in other space-filling cellular structures, e.g. foams [6]) have the combinatorial types of *simple* 3-polytopes. These obey the constraints that two faces meet on at most one edge and exactly three faces meet at each vertex. Similarly, a space-filling three-dimensional microstructure is *simple* if exactly four cells meet at each vertex, three cells meet at each edge, and two cells meet on at most one face.

Many concepts in this article are more naturally described and algorithmically computed by means of the *dual polytope*. For any polytope P, there is a dual polytope P^* such that the faces and vertices of P have
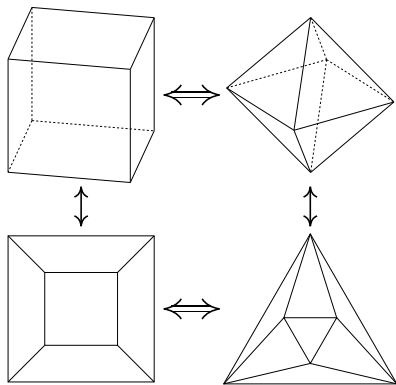

FIG. 3. The relationship of a simple 3-polytope to the corresponding dual simplicial 3-polytope (double arrow), and of a polytope to the corresponding Schlegel diagram (single arrow).
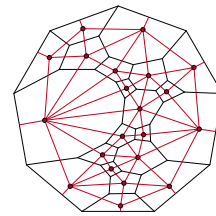

FIG. 4. The Schlegel diagram of a grain and the dual graph of the set of all faces; the dual graph vertex for the back face is not shown.
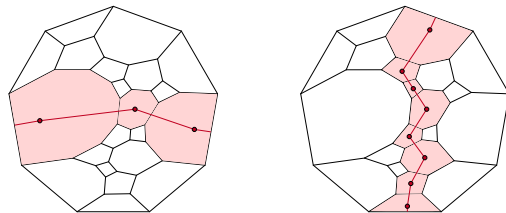

FIG. 5. A 4-belt (left) and a 9-belt (right) of a grain shown on the Schlegel diagram along with their dual graphs. The back face belongs to the belt in both cases.

an incidence-preserving correspondence with the vertices and faces of P^*, respectively. This implies that when P is a simple 3-polytope (three faces meet at every vertex), P^* is a *simplicial* 3-polytope (every face is a triangle), and conversely. Note that the boundary of a simplicial 3-polytope is always a triangulation of the sphere S^2, the *dual triangulation* to the simple boundary of P. As examples, the octahedron is dual to the cube (shown at the top of Figure 3), and the icosahedron is dual to the pentagonal dodecahedron. The tetrahedron is the only simple 3-polytope that is self-dual, and as such it is both simple and simplicial.

While the combinatorial types of the cube and the octahedron are clear from Figure 3, the combinatorial types of more complicated 3-polytopes can be difficult to visualize from the embeddings. The *Schlegel diagrams* at the bottom of Figure 3 are often more convenient to show the combinatorial type of a 3-polytope. This diagram is constructed by projecting the boundary of a polytope onto one of the faces in such a way that vertices not belonging to the face lie inside it, and no two edges cross [7, 8].

All simple 3-polytopes belong to one of three classes, identified by the following characteristics:

- four triangular faces (the tetrahedron),
- more than four faces and no triangular faces,
- more than four faces and some triangular faces.

Truncating any corner of a simple 3-polytope in the first or second classes gives a simple 3-polytope in the third class, and any simple 3-polytope in the third class can be constructed in this way. This suggests the following definition:

Definition 1 *A simple 3-polytope is* fundamental *if it cannot be obtained by truncating a corner of a simple 3-polytope with fewer faces, and is* vertex-truncated *otherwise.*

As described in Section I, the polytopes belonging to physical systems subject to energy minimization often appear to be geometrically round. If some characteristic combinatorial feature of these polytopes could be found, then that would motivate a corresponding notion of combinatorial roundness. In this vein, a round object can be described as having an absence of constrictions, i.e., a belt of any orientation around the object would slide off. The combinatorial analogue of such a geometric constriction uses the notion of a *dual graph*. Given a set of faces, the dual graph contains a vertex for each face in the set, and an edge connects two vertices whenever the corresponding faces share an edge. The dual graph of the set of all faces of an example grain is shown in Figure 4. A combinatorial constriction can now be defined as follows:

Definition 2 *An ℓ-belt of a simple 3-polytope is any set of ℓ faces such that the dual graph of the faces is a cycle (a triangulated circle). A 3-belt is* trivial *if the three faces share a unique vertex, and is* non-trivial *otherwise.*

Figure 5 shows a 4-belt (left) and a 9-belt (right) of the grain in Figure 4, with the faces of the respective belts shaded in red. One of the faces of each of these belts is the back face. Observe that the dual graph of an ℓ-belt is a cycle containing ℓ vertices that are cyclically connected by ℓ edges.

Lemma 3 *The removal of an ℓ-belt from the boundary of a simple 3-polytope leaves one (for a trivial 3-belt) or two connected components that are discs.*

Any vertex-truncated simple 3-polytope has at least one triangular face, and the neighboring faces of such a triangle form a non-trivial 3-belt around the triangle. Perhaps more significantly, a fundamental 3-polytope that is not the tetrahedron can have a non-trivial 3-belt
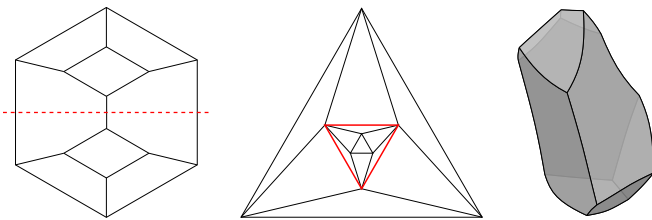
FIG. 6. The Schlegel diagram of the smallest possible fundamental simple 3-polytope with a non-trivial 3-belt (indicated by the dotted red line), the dual triangulation with an *empty triangle* (solid red line), and an example from a three-dimensional evolved microstructure with this combinatorial type.

as well, despite not having any triangular faces; Figure 6 shows the smallest (in terms of number of faces) such example. The severe geometric distortion that accompanies the 3-belt of this polytope suggests the following definition:

Definition 4 *A fundamental simple* 3-*polytope that is not the tetrahedron (i.e., has no triangular faces) is* flag* *if it has only trivial* 3-*belts, and is* severely constricted (sc) *otherwise.*

The term *flag* is usually used in combinatorial topology to describe a simplicial complex K where every complete subgraph in the 1-skeleton (edge graph) of K spans a simplex of K [9, 10]. This means that a flag simplicial complex does not have any *empty faces*, and that every flag simplicial complex can be reconstructed from its 1-skeleton by inserting a face in every complete subgraph of the vertices. The full tetrahedron is the smallest example of a three-dimensional flag simplicial complex; the 1-skeleton is a complete graph on 4 vertices, implying that the complex contains a three-dimensional face (the original tetrahedron). The boundary of the full tetrahedron is a two-dimensional simplicial complex that is not flag, since the 1-skeleton is the same but the three-dimensional face is not included. The smallest example of a two-dimensional flag simplicial complex that triangulates S^2 is the boundary of the full octahedron.

The existence of a non-trivial 3-belt of a simple 3-polytope is closely related to the *connectivity* of the boundary of the dual simplicial 3-polytope. Specifically, the 1-skeleton of a simplicial 3-polytope is 4-connected if, for every pair $\{v, w\}$ of distinct vertices v and w, the 1-skeleton contains four independent paths connecting v and w. For example, the south-pole of the octahedron of Figure 3 can be connected to the north-pole by four independent paths. Observe that there can be no empty triangles in a 4-connected 1-skeleton of a simplicial 3-polytope since only three non-intersecting paths could be routed via the three vertices of an empty triangle. This allows an alternative definition of a flag simplicial 3-polytope via the following lemma (cf. [11]):

Lemma 5 *The* 2-*dimensional boundary complex of a*

simplicial 3-*polytope is flag if and only if its* 1-*skeleton is* 4-*connected.*

The motivation for extending the definition of flag to simple polytopes in Definition 4 is the observation that any flag* simple 3-polytope P is dual to a flag simplicial 3-polytope P^*. That is, if P (except for the tetrahedron) does not have any non-trivial 3-belts, then the 1-skeleton of P^* does not contain any empty triangular faces and is 4-connected.

B. Combinatorial Roundness

As specified in Definition 4, a flag* simple 3-polytope P satisfies a number of restrictive requirements. Since P is fundamental and not the tetrahedron, P cannot have any triangular faces. Since P only has trivial 3-belts, the 1-skeleton of the dual simplicial 3-polytope must be 4-connected. While there is some motivation to consider flag* simple 3-polytopes as combinatorially round, using this as a definition is excessively restrictive for physical systems where simple 3-polytopes evolve by energy minimization. The reason is that a flag* simple 3-polytope acquires a triangular face and briefly becomes vertex-truncated whenever one of the neighboring polytopes is about to disappear as a tetrahedron. More generally, computational results suggest that triangular faces frequently appear and disappear as transitional topological events in material microstructures [3]. Ideally, our definition of combinatorial roundness would be robust to this type of transient event.

One approach is to define combinatorial roundness in such a way to include combinatorial types that are a few vertex truncations away from being flag*. To make this more precise, observe that repeated truncations are locally tree-like. The first truncated vertex can be considered as the root of a tree, and the tree grows whenever one of the newly obtained vertices is truncated. If a different original vertex is truncated instead, this begins a different tree. For the purpose of notation, let $W = \{T_1, T_2, \ldots, T_t\}$ be a collection of t (not necessarily distinct) rooted trees. Since every truncation introduces three new vertices that can be used for further truncations, the T_i are all ternary trees.

Definition 6 *A simple* 3-*polytope P belongs to the class* flag^*_W *or* sc_W *if P is derived respectively from a* flag* *or* sc *simple* 3-*polytope by a sequence of vertex truncations, with the truncation sequence locally represented by the collection of rooted* truncation trees W.

A fundamental 3-polytope F and a collection of truncation trees W do not uniquely specify the derived simple 3-polytope P, since a truncation tree identifies neither the original vertex at which the tree occurs nor the vertex that is truncated when the tree is extended. That W is composed of trees does imply that a simple 3-polytope P is enough to uniquely specify the originating fundamental 3-polytope F, though.
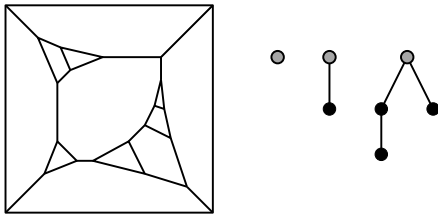
FIG. 7. A simple 3-polytope with 13 faces that is seven truncations away from the cube. The collection of rooted truncation trees is on the right, with a truncation depth of three.

Lemma 7 *Any simple 3-polytope is either fundamental, or can be reduced to a unique fundamental 3-polytope by reversing truncations in any order.*

For example, the simple 3-polytope on the left of Figure 7 is derived from the cube by seven truncations. This can be verified by repeatedly collapsing any one of the remaining triangular faces until the 3-polytope is fundamental.

Let $+r_i$ indicate that T_i is a path (i.e., a tree without branches) with r_i vertices. In particular, the class flag^*_{+1} contains all simple 3-polytopes that are derived from flag* 3-polytopes by a single truncation. Simple 3-polytopes that are derived from flag* 3-polytopes by exactly two truncations fall into two classes, flag^*_{+1+1} and flag^*_{+2}. Examples in the first class have two triangular faces (obtained by truncating two distinct original vertices), while examples in the second class have only one triangular face (obtained by truncating one original vertex and one of the newly introduced vertices). More generally, examples in the class flag^*_{+r} for any positive integer r have only one triangular face. This reinforces that the collection $\{T_1, T_2, \ldots, T_t\}$ of truncation trees provides a more detailed description of the polytope than merely the number of triangular faces [12, 13].

Other significant classes include $\text{flag}^*_{\leq k}$, $\text{flag}^*_{\geq k}$, flag^*_{k}, and $\text{flag}^*_{\geq}$, which are derived from flag* simple 3-polytopes by *at most* k, *at least* k, *exactly* k, and *any number of* truncations, respectively. The classes $\text{sc}_{\leq k}$, $\text{sc}_{\geq k}$, sc_{k}, and $\text{sc}_{\geq}$ for severely constricted simple 3-polytopes are defined similarly. Finally, the *truncation depth* of a simple 3-polytope of type flag^*_W or sc_W is the number of vertices of a longest rooted path in one of the rooted trees in W. For example, the simple 3-polytope in Figure 7 has a truncation depth of three.

The dual relationship of a simple 3-polytope to a simplicial 3-polytope implies that operations on simple 3-polytopes have corresponding operations on simplicial 3-polytopes. Specifically, a vertex truncation of a simple 3-polytope induces a *stacking operation* on the dual simplicial 3-polytope, where a triangle is subdivided by placing a new vertex slightly 'above' the center of the triangle. Let a *stacking tree* be defined such that for any simple 3-polytope P and dual simplicial 3-polytope P^*, the collection of truncation trees $\{T_1, T_2, \ldots, T_t\}$ of P is identical to the collection of stacking trees $\{S_1, S_2, \ldots, S_t\}$ of P^*.

Then the truncation depth of P and the *stacking depth* of P^* are always the same.

Since the tetrahedron is the unique fundamental simple 3-polytope with triangular faces, some specific terminology is introduced to identify the 3-polytopes derived from the tetrahedron.

Definition 8 *A simple (simplicial) 3-polytope is stacked* (stacked) if it can be obtained from a tetrahedron by a sequence of vertex truncations (stacking operations).*

The flag octahedron with six vertices is the smallest simplicial 3-polytope that is not stacked. There is always a vertex of degree three on the boundary of a stacked simplicial 3-polytope (e.g., the vertex most recently introduced by a stacking operation), and all vertices of the octahedron have degree four.

A simple 3-polytope that is at most k truncations away from a flag* simple 3-polytope is said to be *k-close to flag**, and a simple 3-polytope that is at most k truncations away from the tetrahedron is said to be *k-close to tetrahedral*. This allows a combinatorial roundness to be defined for simple 3-polytopes as follows:

Definition 9 *A simple 3-polytope is* combinatorially k-round *and belongs to the class* $\text{round}_{\leq k}$ *if it is k-close to flag* or k-close to tetrahedral.*

There is an analogous definition of the class $\text{round}_{\leq k}$ for simplicial 3-polytopes, where k-close to flag and k-close to tetrahedral bound the number of stacking operations rather than the number of vertex truncations. Our intention is to provide preliminary evidence that the class $\text{round}_{\leq k}$ for small values of k connects the combinatorial structure of a grain in a material microstructure to its geometric shape (being round in the sense of small surface area), and thereby to the frequency of its combinatorial type in energy-minimizing structures.

Finally, triangulations of the boundary 2-spheres of simplicial 3-polytopes with up to 23 vertices have been enumerated by Brinkmann and McKay [14], as well as all examples with minimal vertex-degree at least four and all 4-connected flag examples with up to 27 vertices (Table II). Explicit lists of the triangulations with up to 14 vertices can be found online [15]. These will be used in Section III A to show that $\text{round}_{\leq k}$ is a small subset of all triangulations with a given number of vertices, particularly for small values of k.

III. COMPUTATIONAL RESULTS

A. Microstructure Evolution

Grain growth simulations generally assume that the grain boundary energy and mobility are constants, and that capillary pressure drives grain boundary motion. For this model, a generic geometric initial condition converges to a statistical steady state where the faces are
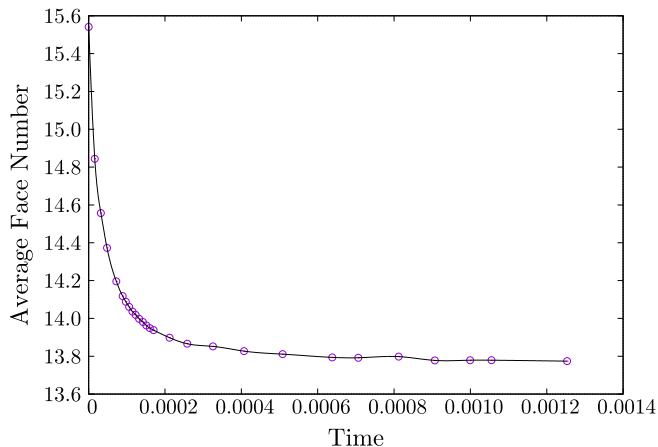
FIG. 8. Evolution of the average number of faces per grain in time from a Poisson–Voronoi initial condition with constant grain boundary energy and mobility.

FIG. 10. Evolution of the fraction of grains that are flag* in time from a Poisson–Voronoi initial condition with constant grain boundary energy and mobility.
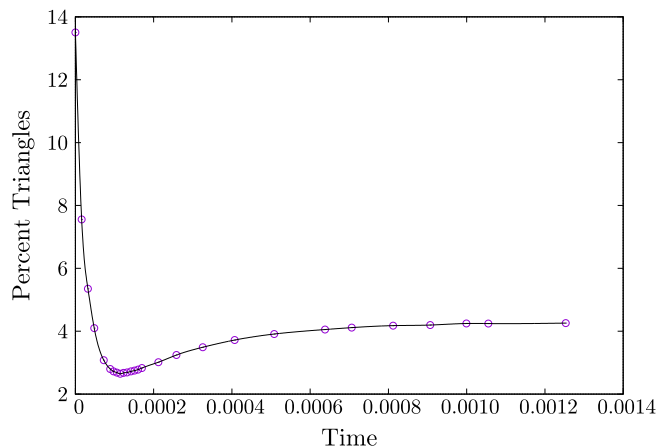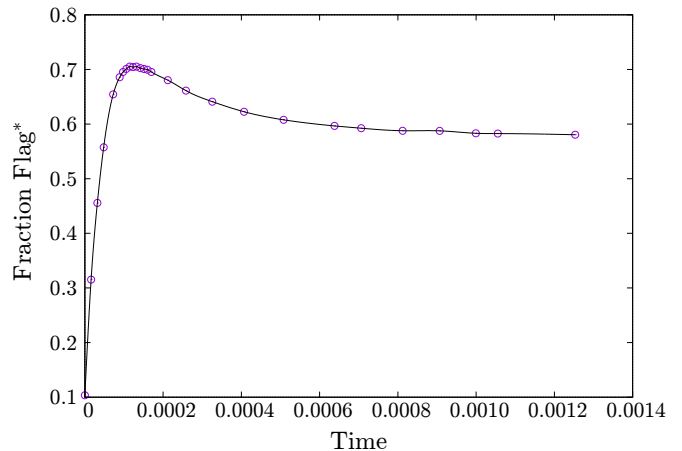

FIG. 9. Evolution of the percent of triangular faces in time from a Poisson–Voronoi initial condition with constant grain boundary energy and mobility.

curved and boundary motion continues but dimensionless statistical quantities are constant [4]. The average number of faces per grain in this steady state is 13.769 ± 0.016 [3, 4], though a precise justification of this value is not known.

One of the main purposes of this paper is to more closely analyze the grain growth process and the induced dynamics on the space of topological types using the terminology introduced in previous sections. The specific numerical model used in the following is explained in detail elsewhere [3]. Time is always expressed in dimensionless units of $1/m\gamma$, where m and γ are the constant grain boundary mobility and energy per unit area, respectively.

Consider a grain growth simulation initialized with a Poisson–Voronoi microstructure that has an average of about 15.535 faces per grain [16]. Figure 8 shows that the average number of faces per grain is (effectively) monotone decreasing in time, and converges to the steady state

value of 13.769 [3]. However, the percentage of faces that are triangles (Figure 9) and the fraction of grains that are flag* (Figure 10) show significant initial transients before converging to the steady state values. The minimum in Figure 9 and the maximum in Figure 10 occur at the same time of 0.000115. That these should coincide is reasonable since grains without triangles are fundamental (flag* or severely constricted), and the population of severely constricted grains is expected to be small.

Let the initial microstructure be called the *Poisson–Voronoi* condition, the microstructure in the statistical steady state be called the *Evolved* condition, and the microstructure at time 0.000115 be called the *Round* condition. The measurements in the following sections are made using three data sets, one for each condition:

- The Poisson–Voronoi data set (V-268402) was constructed from 268,402 seeds in the unit cube with periodic boundary conditions.
- The Evolved data set (E-268402) was obtained by taking 25 Poisson–Voronoi microstructures, each containing 100,000 grains, for a total of 2,500,000 initial grains. These were allowed to evolve by normal grain growth until a total of 269,555 grains remained. The data set contains the 268,402 grains that were polytopal (the other 1153 were degenerate, as described in Section IV).
- The Round data set (R-268402) was constructed from the same simulation as the Evolved data set by sampling 268,402 polytopal grains from the microstructure at time 0.000115.

As justification for the behavior in Figures 9 and 10, observe that the average grain size increases during the process of grain growth, requiring some grains to shrink and disappear. Since the microstructure is roughly equiaxed, reducing the volume of a shrinking grain reduces the edge lengths and face areas of the grain as well. This induces a sequence of topological operations neces-

sary to maintain the connectivity of the microstructure. From the standpoint of a shrinking grain, a vanishing edge is replaced by a different edge that exchanges the neighbors of the bounding vertices (an edge flip), and a vanishing face is replaced by a single vertex (a reverse truncation). From the standpoint of the surrounding grains, the same operations can involve edge flips, truncations, or reverse truncations. This makes the fraction of triangular faces depend on the relative rates of the interacting topological operations in a complicated way. That said, every shrinking grain that remains polytopal must pass through the tetrahedron before vanishing, and the transient population of tetrahedral grains places a lower bound on the fraction of triangular faces present in the microstructure.

For the Poisson–Voronoi data set, 13.503% of the faces are triangles, none of the grains are tetrahedral, 0.01% of the grains are stacked*, and 10.36% of the grains are flag* (Table IV). For the Round data set, 2.647% of the faces are triangles, 0.05% of the grains are tetrahedral, 0.25% of the grains are stacked*, and 70.52% of the grains are flag* (Table V). This is interpreted to mean that the capillary pressure characteristic of grain growth drives the grains to be more geometrically round and reduces the initially high fraction of triangular faces, while the relative absence of vanishing grains does not bound the fraction of triangular faces from below. For the Evolved data set, 4.259% of the faces are triangles, 0.14% of the grains are tetrahedral, 0.69% of the grains are stacked*, and 58.05% of the grains are flag* (Table VI). The population of shrinking and vanishing grains has increased relative to the Round data set, eventually reaching a condition where the number of triangular faces generated by shrinking grains is equal to the number of triangular faces consumed by the action of capillary pressure.

This suggests that the Round microstructure is characterized by grains with unusually stable topology, appearing after the relaxation of the Poisson–Voronoi microstructure and before the appearance of a substantial population of vanishing grains. The Round microstructure is further notable for having an average of 14.036 faces per grain, only slightly above the 14 faces per grain in Kelvin's equal volume foam [17]. While Kelvin's foam was long thought to have the least area of any equal volume foam, the Weaire–Phelan foam is more economical with an average of only 13.5 faces per grain [18]. Kusner and Sullivan still conjecture that Kelvin's foam is optimal as an equal volume equal pressure foam [19], though.

Real microstructures, for example steels, depart from the above idealized grain growth model in a number of respects. The presence of multiple phases, concentration gradients, plastic strain around martensitic lathes, and orientation- and concentration-dependent grain boundary properties are all known to affect the evolution of the microstructure, though our understanding of these changes is vague due to experimental and theoretical limitations. Fabricating a microstructure in the Round condition would further require that the initial microstruc-
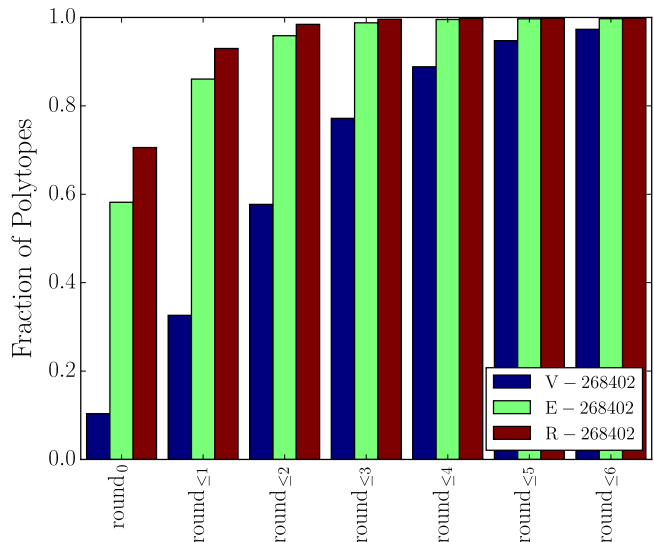

FIG. 11. Fraction of round $_{\leq k}$ grains in the Poisson–Voronoi, Evolved and Round microstructures.

ture be in the Poisson–Voronoi condition, and this is not always a reasonable approximation for samples solidified from the liquid. Nevertheless, an approximate initial condition could be fabricated by dispersing fine insoluble particles in the liquid to induce uniform heterogeneous nucleation of the solid phase, resulting in a roughly equiaxed microstructure with approximately planar grain boundaries. This should have the same properties as the Poisson–Voronoi data set considered here, namely, an excess of triangular faces and a relative absence of tetrahedral grains. A short anneal would still presumably reduce the average number of faces per grain, despite the complications mentioned above. An interesting experiment would be to quench the sample when the average number of faces per grain is close to 14 (as an approximation to the Round microstructure), both to investigate the topological properties of the grains and whether this topology imparts any enhanced mechanical properties.

Whereas Figure 10 shows the fraction of grains that are flag* as a function of time, the class round$_{\leq k}$ of all combinatorially k-round grains is more robust to the appearance of transient triangular faces. Table VII and Figure 11 give the percentages of k-round grains in the three data sets for $0 \leq k \leq 6$. This is already sufficient to include almost all of the grains since 97.32%, 99.86% and 99.72% of the polytopal grains in the Poisson–Voronoi, Evolved and Round data sets, respectively, are 6-round. Figure 12 shows that the percentage of round$_k$ grains decays roughly exponentially for higher values of k, though the reason for this rate of decay is unknown.

That the Voronoi data set consistently has fewer k-round grains for $0 \leq k \leq 6$ suggests that normal grain growth strongly supports the formation of combinatorially round grains. Further evidence for this claim is found by comparing the three data sets to the set of all
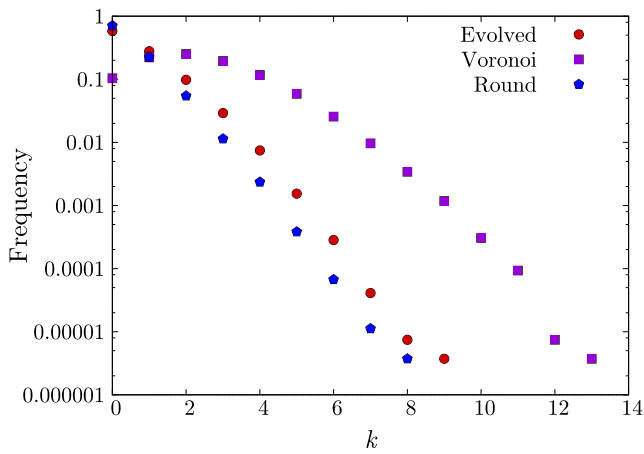
FIG. 12. The frequencies of round_k grains for the Poisson–Voronoi, Round and Evolved data structures.
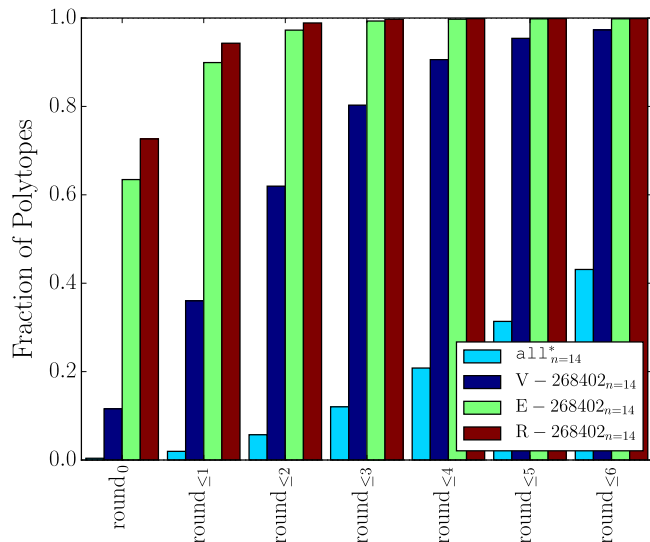

FIG. 13. Fraction of $\mathrm{round}_{\leq k}$ grains in the Poisson–Voronoi, Evolved and Round microstructures, restricted to $n = 14$ faces, and compared to all possible grains with $n = 14$ faces.

simple 3-polytopes with few faces. As mentioned in Section II B, triangulations of the 2-dimensional sphere with up to 23 vertices have been enumerated by Brinkmann and McKay [14]; refer to Table II for select statistics. Triangulations with up to 14 vertices are further classified in Table III as stacked, flag, flag_{+1}, flag_{+1+1}, flag_{+2}, $\mathrm{flag}_{\geq 3}$, sc^*, sc^*_{+1} or $\mathrm{sc}^*_{\geq 2}$. This table indicates that the fraction of flag examples decreases with the number of vertices n, and similarly that the fraction of examples in the class $\mathrm{flag}_{\leq k}$ decreases with n for a given value of k.

Since the Poisson–Voronoi, Round and Evolved data sets all have face averages close to 14, we compare these with the set $\mathtt{all}^*_{n=14}$ of simple polytopes that are dual to the set $\mathtt{all}_{n=14}$ of all triangulations of the 2-sphere with 14 vertices. The latter includes 339,722 distinct

simplicial 3-polytopes, only 0.40% of which are flag. Figure 13 shows the fractions of k-round simple polytopes in $\mathtt{all}^*_{n=14}$ and the corresponding fractions of k-round grains with 14 faces in the Poisson–Voronoi, Round and Evolved data sets. We infer that although k-round grains are rare among all possible grains for small k, the Poisson–Voronoi, Round and Evolved microstructures consist almost entirely of these grains.

Alternatively, consider the grains that do not belong to k-round for small k. From Table VII, 43.11% of all possible grains with 14 faces are 6-round, and the 56.89% remaining necessarily belong to the types $\mathrm{flag}^*_{\geq 7}$ or $\mathrm{sc}_{\geq}$. By comparison, only 2.68%, 0.28% and 0.14% of the grains with 14 faces in the Poisson–Voronoi, Evolved and Round data sets, respectively, are $\mathrm{flag}^*_{\geq 7}$ or $\mathrm{sc}_{\geq}$. That is, grains of the types $\mathrm{flag}^*_{\geq 7}$ or $\mathrm{sc}_{\geq}$ are rare in the space-filling Poisson–Voronoi, Evolved and Round microstructures; we conjecture that this is true of generic space-filling microstructures as well.

B. Geometric Roundness

The motivation for our study of the combinatorial types of grains is that there should exist some combinatorial property that is positively correlated with the geometric roundness of a grain. That the combinatorial roundness as defined in Section II B should satisfy this criterion is perhaps not obvious. To the contrary, starting with a convex polyhedron and repeatedly truncating the vertex with the highest angular deficit would appear to make the polyhedron more spherical. That is, round_k for any $k > 0$ could contain grains that are *more* geometrically round than those in round_0, not less as suggested in Section III A.

This reasoning does not account for the effect of the vertex truncations on the surrounding microstructure, though. Specifically, for an isotropic boundary energy the system evolves to reduce the total boundary area, with the consequence that the tangents to the edges at a vertex always meet at the tetrahedral angle. Introducing vertices on the surface of a grain by vertex truncation can then increase the grain's surface area to volume ratio if the adjoining faces acquire a negative curvature to satisfy the edge constraint.

Of course, the natural recourse to discern the relationship of combinatorial roundness to geometric roundness is direct measurement. A standard measure for geometric roundness of a 3-dimensional object is the dimensionless *isoperimetric quotient*

$$Q = 36\pi V^2/S^3, \tag{1}$$

where V is the volume and S is the surface area of the object. The isoperimetric quotient is confined to the interval $0 \leq Q \leq 1$, with values of 1 for the sphere, 0.755 for the dodecahedron, 0.524 for the cube, and 0.302 for the tetrahedron (all regular). That is, the value increases with geometric roundness.
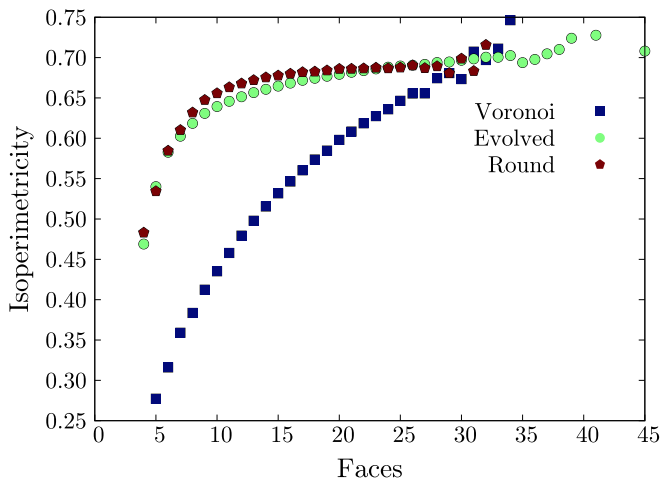
FIG. 14. The average isoperimetricity of grains with a given number of faces for the Poisson–Voronoi, Round and Evolved microstructures.
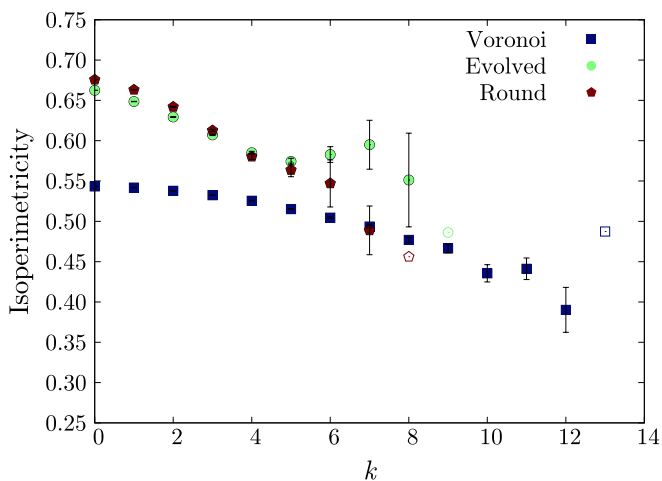

FIG. 15. The average isoperimetricity of round$_k$ grains for the Poisson–Voronoi, Round and Evolved data structures. Error bars are the standard error of the mean, and classes with a single grain are indicated by an open marker.

Figure 14 shows the average isoperimetric quotient of the grains as a function of the number of faces for the Poisson–Voronoi, Round and Evolved microstructures. The average reliably increases with the number of faces, with the plateau for the Round and Evolved microstructures possibly related to an upper bound for uniform space-filling cellular structures. Grains with fewer than 23 faces (the vast majority) consistently have the highest average isoperimetric quotients in the Round microstructure and the lowest in the Voronoi microstructure, consistent with the fractions of round$_{\leq k}$ grains in Figure 11. The scatter for the highest number of faces is a consequence of sampling error, though the Evolved microstructure does contain a population of grains with many faces and high isoperimetric quotient that is absent from the other microstructures.

Figure 15 more directly addresses the central concern of this section, namely, the correlation of the average isoperimetric quotient of round$_k$ grains with k. That the isoperimetric quotient generally decreases with k indicates that the combinatorial roundness and geometric roundness are indeed positively correlated, as hypothesized in Section II. The obvious exception is the increasing average isoperimetric quotient for grains in the Evolved microstructure that are $5 \leq k \leq 8$ vertex truncations away a fundamental grain. A more detailed investigation reveals that this population mainly consists of two groups, a group of stacked* grains with $n \leq 13$ faces and of a group of truncated flag* grains with $n \geq 20$ faces. The first group has a much smaller average isoperimetricity (0.491 ± 0.065) than the second (0.665 ± 0.037), which along with the small population size explains the increase in the standard error of the mean.

An explanation for the existence of the group with $n \geq 20$ faces and the shift in the average isoperimetic quotient begins with the observation that the Evolved microstructure contains some grains that are significantly larger than the average grain, and that often continue to grow and consume the surrounding structure. Since the microstructure has a well-defined average edge length, these grains are expected to have more faces than the average grain. Since the surrounding grains are shrinking and transitioning through tetrahedra, more of the faces are expected to be triangles than for the average grain. That is, the largest grains are overrepresented in the Evolved microstructure for $5 \leq k \leq 8$ in Figure 15, increasing the average isoperimetric quotient. This explanation is supported by the intimation of a similar deviation for the Round microstructure where the population of largest grains is not yet fully developed.

C. Grain Classes and Error Analysis

The dependence of the frequencies of the simple polytope classes defined in Section II B on the system evolution is considered further in Figure 16, which shows the frequencies of several simple polytope classes as functions of the number of faces n in the Poisson–Voronoi, Round, and Evolved microstructures. The black curves are the distributions of the number of faces, and show that the system evolution on average reduces the number of grains with many faces and increases the number of grains with few faces. This is consistent with the average number of faces per grain being 15.535, 14.036, and 13.769 for the Poisson–Voronoi, Round, and Evolved microstructures, respectively.

Figure 16 further shows a noticeable decrease in the flag*$_{+1+1}$ and flag*$_{\geq 3}$ grain populations from the Poisson–Voronoi to the Round microstructure, with a corresponding increase in the population of flag* grains. Since a 0-round grain is necessarily either tetrahedral or belongs to the class flag*, the increase in the population of flag* grains is consistent with the Round microstructure hav-
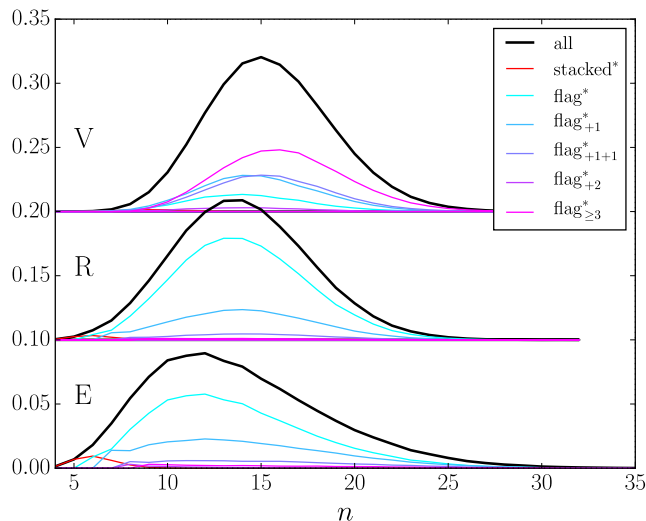
FIG. 16. Frequencies of various grain classes in the Poisson–Voronoi (V), Round (R), and Evolved (E) microstructures, where n is the number of faces. Values for the Poisson–Voronoi and Round microstructures are vertically offset by 0.20 and 0.10, respectively.
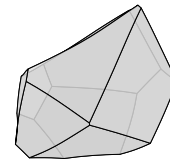

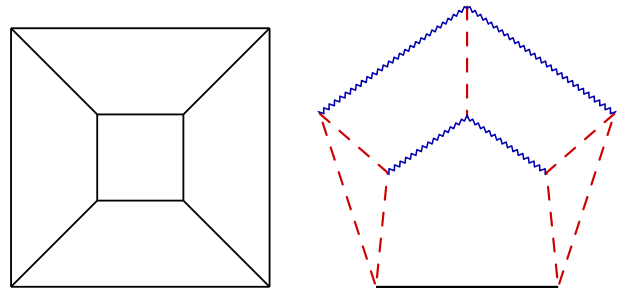FIG. 17. Dodecahedron from the Evolved data set with several short edges.

FIG. 18. Schlegel diagrams of the two polytopes with six faces. The flip of a bold edge gives the other polytope, the flip of a zigzag edge gives the same polytope, and the dashed edges are non-admissible.

ing more 0-round grains than the Poisson–Voronoi microstructure in Figure 11. Note also that grains of type flag$^*_{+1+1}$ are consistently more frequent than grains of type flag$^*_{+2}$ (Tables IV, V and VI). The reason for this is likely combinatorial. Given a flag* grain, a grain of type flag$^*_{+1+1}$ is obtained by truncating any two of the original vertices. A grain of type flag$^*_{+2}$ is only obtained if the second truncated vertex is one of the three vertices newly introduced by the first truncation.

There are three further significant changes in the frequencies of simple polytope classes as the system evolves from the Round to the Evolved microstructure. First, non-negligible populations of stacked* and flag$^*_{+1}$ grains with small numbers of faces appear. These grains are likely in the process of losing faces before vanishing, and correspond to a transient population that is not substantially present in either the Poisson–Voronoi or Round microstructures. Second, the frequency of flag* grains is somewhat reduced overall, with the distribution skewed toward small n. The significance of the skewness is not known, but the reduced frequency of flag* grains is consistent with the Evolved microstructure having fewer 0-round grains than the Round microstructure in Figure 11. Third, the Evolved microstructure has more grains (and in particular flag* grains) with $n \geq 22$ faces than the Round microstructure. These grains represent heterogeneities that could degrade certain mechanical properties, and provide further motivation to investigate the properties of materials that approximate the Round microstructure.

The preceding analysis of combinatorial types presupposes that the topology of a grain is well-defined. The example grain in Figure 17 suggests that arbitrarily small

perturbations to a grain's geometry could induce topological transitions that change the grain's combinatorial type without changing the number of faces, though. This raises a reasonable question about the independence of the statistics reported in this section to errors introduced by implementation details and finite precision arithmetic.

Consider the effect of a fixed rate of topological edge errors per grain on the frequency of round$_k$ grains. Starting from the Evolved data set with 268,402 grains, every grain is subjected to a fixed number of edge flips selected uniformly at random from the set of admissible edges (ones that do not give a degenerated grain). Note that the presence of combinatorial symmetries means that distinct flips can sometimes give the same combinatorial type, or even leave the combinatorial type unchanged. For example, the only two simple 3-polytopes with six faces are the cube with p-vector $(0, 6, 0)$ and the unique simple 3-polytope with p-vector $(2, 2, 2)$, where the p-vector is described in Appendix A. The Schlegel diagrams of these polytopes are given in Figure 18. The flip of any edge of the cube gives the second polytope. For the second polytope, the flip of any of four edges does not change the polytope, the flip of one edge gives the cube, and the remaining seven edges are non-admissible. There is generally more variability for grains with more faces.

Figure 19 shows the effect of the above procedure on the frequencies of round$_k$ grains in the Evolved data set, along with the corresponding frequencies for the Poisson–Voronoi and Evolved data sets. Observe that the frequencies do not change substantially for one edge error per grain. Since the fraction of edges in the Evolved data set with less than one-tenth the average length is
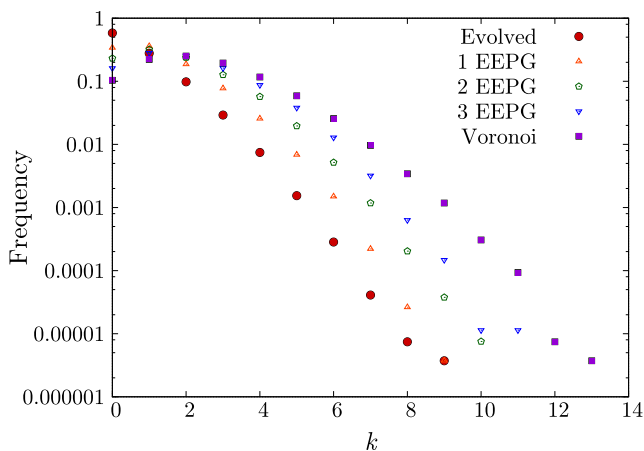
FIG. 19. The frequencies of round$_k$ grains in the Poisson–Voronoi and Evolved data sets, and for grains in the Evolved data set after flipping a fixed number of edges per grain. EEPG stands for edge errors per grain.

about 0.027 and a grain in the Evolved microstructure has about 35 edges [4], there is roughly one error candidate per grain. That said, this is a very conservative estimate, the actual average number of edge errors per grain is likely much less than one, and this source of error is unlikely to significantly change the reported statistics. We take this opportunity to further observe that increasing the number of edge errors per grain to two or three causes the frequencies of round$_k$ grains to move in the direction of those of the Poisson–Voronoi data set — which is still far from randomly picking grains from the set of all grains with few faces.

D. Flag* Grains

The above sections define several combinatorial classes of simple polytopes and consider the frequencies of grains belonging to those classes in a space-filling microstructure evolving by normal grain growth. This section is instead concerned with a refined analysis of the class of flag* simple 3-polytopes and the extent to which the frequency of a particular combinatorial type can be predicted from combinatorial information alone. The present proposal is restricted to flag* simple 3-polytopes since this is the main class considered in the previous sections, and the topology of these polytopes is relatively well constrained.

As explained in Section II A, one of the characteristics of a flag* simple 3-polytope is the absence of non-trivial 3-belts. Let the notation $k:\ell:m$ indicate that a polytope with $k + \ell + m$ faces has an ℓ-belt, and that the removal of this belt leaves two disks with k and m faces where $k \leq m$. Then the property of flag* simple 3-polytopes mentioned above is equivalent to simple 3-polytopes with $n \geq 6$ faces not having any 3-belts except for ones of the

type $0:3:(n-3)$.

Intuitively, a belt of type $k:\ell:m$ for fixed ℓ imposes a constriction on the polytope that becomes increasingly severe with increasing k. For example, a cube has a 4-belt of type $1:4:1$ and is reasonably described as unconstricted, while a simple 3-polytope with a belt of type $6:4:6$ is likely constricted similarly to the grain in Figure 6. This motivates the following definition:

Definition 10 *A flag* simple 3-polytope P with n faces has* split type $k:\ell:m$ *for a given $\ell \geq 4$ if k is the largest integer (with $k \leq m$) such that P has an ℓ-belt of type $k:\ell:m$. If P does not have an ℓ-belt, it is said to have* split type $0:\ell:(n-\ell)$.

This definition induces a corresponding notion of split-type for the dual simplicial 3-polytope P^*. Specifically, P^* has split type $k:\ell:m$ if k is the largest integer such that P^* has a cycle of length ℓ that, when removed, separates the triangulation into two components with k and m vertices.

A simple 3-polytope with a non-trivial 3-belt is either vertex-truncated or severely constricted, and is excluded from the present analysis. The most severe possible constriction of a flag* simple 3-polytope is therefore from a non-trivial 4-belt. The present analysis considers only 4-belts for simplicity, though a more complete analysis would likely include information concerning ℓ-belts for arbitrary ℓ (where the existence of a non-trivial ℓ-belt with $\ell \leq 5$ is guaranteed by Equation A1 in Appendix A). Given this restriction, the notation $k:4:m$ is abbreviated to $k:m$ and the phrase 'split type' refers to 4-belts in the following.

Table VIII lists the split types of all flag triangulations with up to $n = 14$ vertices. The corresponding numbers of grains with every observed split type in the Poisson–Voronoi, Round and Evolved data sets are reported in Tables IX–XI, respectively. The notable absence of split types $1:3$ and $0:9$ in Table VIII implies that flag* grains with these split types are forbidden. For example, a flag* grain with split type $0:9$ would necessarily have 13 faces, none of which could be 3-gons or 4-gons, and would have the p-vector $(0, 0, 12, 1)$ that is forbidden by Equation A2 [20, p. 271].

Among all flag triangulations with 14 vertices, the split types $5:5$, $4:6$, $3:7$, $2:8$, and $1:9$ occur with the strictly decreasing frequencies 40.83%, 19.23%, 17.32%, 15.40%, and 7.15%, respectively. This is contrary to the trend observed for our space-filling structures in Tables IX–XI, where the frequency of grains with 14 faces and split type $k:m$ generally decreases with increasing k (consistent with the motivation for Definition 10). For example, the frequencies of flag* grains with 14 faces and split type $5:5$ are only 8.02%, 2.38% and 2.06% for the Voronoi, Round, and Evolved microstructures, respectively.

A flag* simple 3-polytope does not have any truncated vertices by definition. A flag* simple 3-polytope with a 4-gon face admits a 4-belt around that face, and therefore has split type $k:m$ with $1 \leq k$. As a consequence:

Lemma 11 *A flag* simple 3-polytope of split type* $0:m$ *has no 3-gon or 4-gon faces.*

By Equation A1, a flag* simple 3-polytope with split type $0:m$ has at least 12 faces; the boundary of the dodecahedron is the unique flag* simple 3-polytope with split type $0:8$ and 12 faces. The next smallest example is the unique flag* simple 3-polytope with split type $0:10$ and 14 faces. Since the average number of faces per grain in the Poison–Voronoi, Round and Evolved data sets is less than or equal to 15.535 (and since initially the fraction of flag* examples is small in the Poison–Voronoi data set), flag* simple 3-polytopes with split type $0:m$ and more than 14 faces should be infrequent in these or any other generic microstructure. A notable example of a non-generic microstructure is the Weaire–Phelan foam, which consists of the two cell types with split types $0:8$ and $0:10$ and has an average of 13.5 faces per grain [19]. Note that it is not possible to tile space with only the dodecahedron — this would yield the notorious 120-cell with positive curvature. Decompositions of non-isotropic spaces $\Sigma^2 \times S^1$ (with Σ^2 any closed surface) are discussed elsewhere [21].

We now consider four prominent species of fundamental grains, the tetrahedron (the smallest fundamental grain), the cube (the smallest flag* grain), the dodecahedron (the smallest flag* grain of split type $0:m$) and the set of all flag* grains of split type $0:m$. The fractions of these four species are shown in Figure 20 as functions of time, starting from the Poisson–Voronoi microstructure and ending with the Evolved microstructure. The gradual increase in the fraction of tetrahedra is caused by a higher initial rate of grains losing faces and transitioning to tetrehedra than of tetrahedra losing faces and vanishing. The fraction of tetrahedra stabilizes in the Evolved microstructure since these two processes necessarily occur at the same rate in the steady state. The fractions of dodecahedra and grains with split type $0:m$ peak at time 0.000212, with 0.108% and 0.287% of grains being of these types, respectively. Note that this is significantly after the point where the fraction of flag* grains peaks and the Round microstructure is identified. The cause of the abrupt shoulder in the fraction of cubes is unknown.

The above examples indicate that combinatorial information alone is not generally sufficient to predict the frequency of a particular flag* simple 3-polytope; Figure 20 shows that the frequency of cubes changes significantly from the Poisson–Voronoi to the Evolved microstructure. More extreme examples are provided by the Kelvin foam and the Weaire–Phelan foam. Kelvin's foam consists of a single cell (the truncated octahedron) with six square faces and eight hexagonal faces. The Weaire–Phelan foam contains two types of cells with significant numbers of pentagonal faces. Since the distributions of cell types for these two foams are disjoint, there cannot be any function that precisely describes the frequency of combinatorial types in *all* space-filling cellular structures.

Instead, we propose a penalty function that effectively bounds the frequency of a given flag* simple 3-polytope
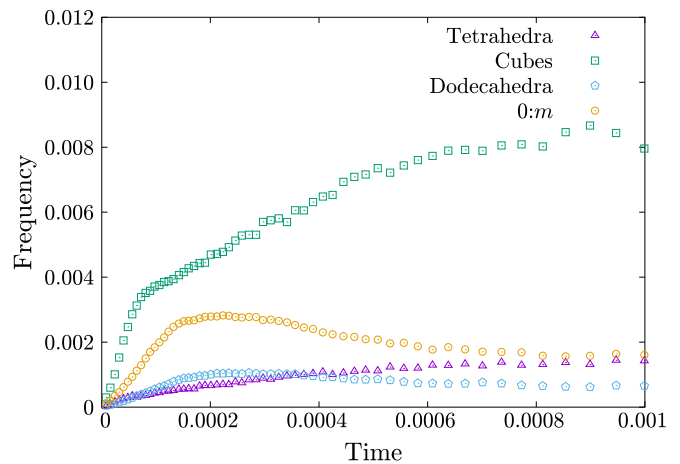

FIG. 20. Percentage of tetrahedra, cubes, dodecahedra, and grains of type $0:m$ over time.

from above. Intuitively, the penalty should increase with the number of faces, with the severity of the constriction by 4-belts, and with the number of 4-belts. One function with these properties follows.

Definition 12 *The* penalty value *of a flag* grain with n faces is*

$$\mathcal{P} = n \sum_k x_k k(n-k-4), \qquad (2)$$

where x_k is the number of 4-belts of type $k:(n-k-4)$.

The penalty function sums over all 4-belt types of a flag* grain, with the sum weighted by the numbers of faces. Figure 21 shows flag* grains with frequencies of at least 0.00001 in the Evolved microstructure as a function of their penalty value. Flag* simple 3-polytopes with split type $0:m$ have penalty value 0, but are not frequent. The largest value for p that we observed in the Evolved microstructure is 21,514 for a grain with 31 vertices. The occurrence of such a grain is most likely due to a *long tail effect* of the statistics — while any individual grain with many vertices and high penalty value will be very infrequent, there are many such possible flag* grains from which some individual grains are sampled. As intended though, the penalty function does appear to give a reasonable upper bound on the frequency of a given flag* simple 3-polytope, at least for this particular microstructure. A more accurate and general penalty function would likely use additional information concerning belts of other lengths, the number of vertex-truncations the polytope is away from a fundamental polytope, and potentially the order of the symmetry group.

With regard to the symmetry group, grains in the Poisson–Voronoi, Evolved, and intermediate microstructures generally have no *geometric* (reflectional or rotational) symmetries at all. For the Poisson–Voronoi case this immediately follows from a general position argument for the (random) normal vectors of the faces of
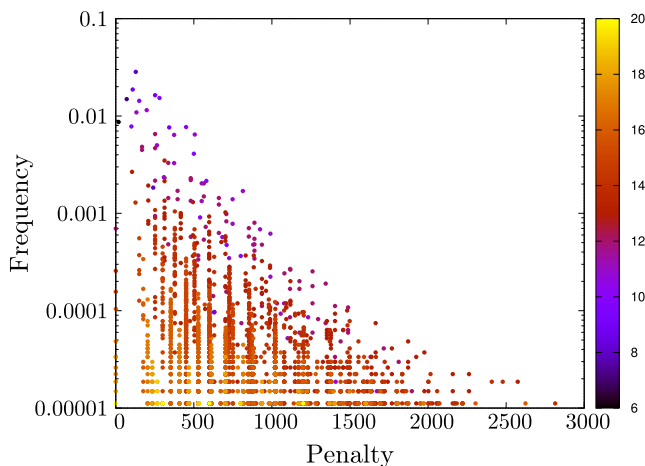
FIG. 21. Flag* grains with frequencies of at least 0.00001 in the Evolved microstructure as a function of penalty value. Color indiates the number of faces.
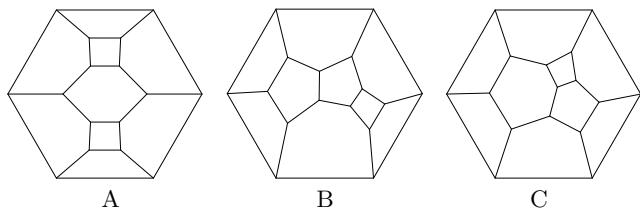

FIG. 22. Three grains A, B, and C with the same p-vector $(0,4,4,2)$.

FIG. 23. Fractions of the three grains with p-vector $(0,4,4,2)$ over time.

the individual simple 3-polytopes, forcing all edges of the polytopes to have different lengths and therefore destroying geometric symmetries. For the Evolved and intermediate cases, the edges and the faces of grains (in simulations and experiments) are curved, presenting a further obstacle to geometric symmetries.

That said, it has been observed "that the most frequent grain *topologies* [emphasis added] in grain growth microstructures are substantially more symmetric than the corresponding ones for Poisson–Voronoi microstructures" [5]. This follows from grains in the Evolved microstructure having on average fewer faces and fewer triangular faces than grains in the Poisson–Voronoi microstructure. By Equation A1, $\frac{1}{n}(p_3+p_4+\dots) = 6-\frac{12}{n}$ for any simple 3-polytope with n faces and p-vector $(p_3, p_4, \dots)$. If n is small and $p_3 = 0$, then $p_k \neq 0$ for large k is not possible. Hence, the most frequent grains will naturally have only 4-gons, 5-gons, and 6-gons, giving them a higher chance of being combinatorially symmetric; see [22] for a complete list of the examples with $n \leq 10$ along with their symmetry groups.

As one set of examples, consider the three simple 3-polytopes A, B, and C in Figure 22, each with 10 faces and p-vector $(0,4,4,2)$. Figure 23 shows that at all times during the evolution, type A is the least frequent and type C is roughly twice as frequent as type B; in fact, type C is the most frequent type of all grains with 10 faces in the
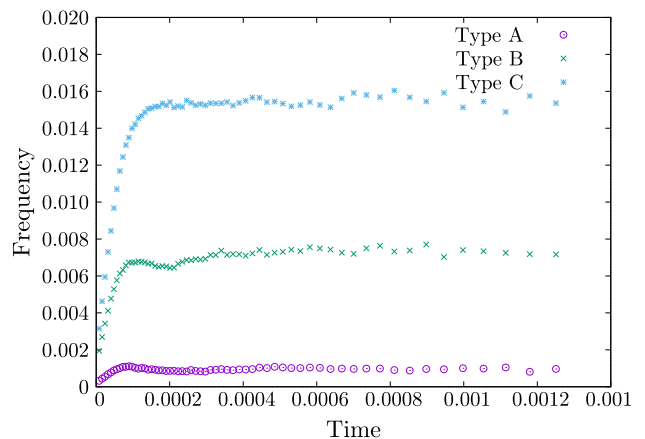
Evolved microstructure. Type A has a symmetry group of order 8, while types B and C have symmetry groups of order 2. That is, the symmetry group seems to be related to frequency of the type, but is not sufficient to distinguish types B and C.

These differences can instead be explained by the measures of combinatorial roundness considered above. Type C has no belts of type $3\!:\!4\!:\!3$, is the most round of the three examples, and is the most frequent one. Type A has two (orthogonal) belts of type $3\!:\!4\!:\!3$, while B has only one. This makes A the most constricted and the least frequent of the three, despite being the most symmetric. Note that this situation is more succinctly described in terms of the penalty values of the three types. The penalty values of types A, B, and C are 380, 290, and 280 respectively. The larger the penalty value, the lower the frequency of the type.

Observe that predicting the frequency of a combinatorial type instead of an upper bound on the frequency would require information about the compatibility of that type with the surrounding microstructure. Consider the three simple 3-polytopes K, L, and M illustrated in Figure 24, each with 14 faces and p-vector $(0,6,0,8)$. Note that K is the Kelvin cell, which can be used to tile space. None of these types appears often at any point during grain growth. This can be understood as a consequence of the absence of 5-gons, which are the most frequent face type. Since every face is shared by two grains, a simple 3-polytope without 5-gons is unlikely to be compatible with the faces presented by the surrounding microstructure; indeed, the most frequent grain with 14 faces in the Evolved microstructure has p-vector $(0,1,10,3)$. Similarly, the disorder of the microstructure makes combinatorial types with only 5-gons (dodecahedra) rare, despite these types being highly symmetric and combinatorially round. The preference of combinatorially round grains that approximate the average p-vector is another property that could be encoded in a generalized penalty function.
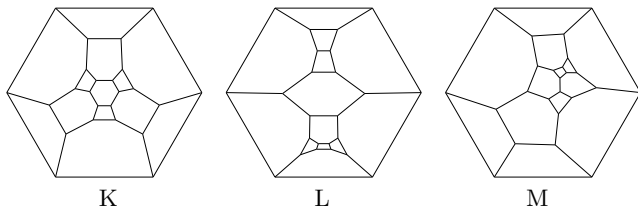
FIG. 24. Three grains K, L, and M with the same p-vector $(0, 6, 0, 8)$.

IV. DEGENERATE AND EXTREMAL GRAINS

Not all of the grains in grain growth microstructures are polytopal, i.e., a small fraction of them cannot be realized as the boundaries of three-dimensional polytopes with straight edges and planar faces. Such grains are said to be *degenerate*. Degenerate grains occur when one of the faces is a 2-gon, as for the grains in Figure 25, or when two faces share more than one edge, as for the grains in Figure 26. Note that, with the exception of the trihedron in Figure 25(a), the presence of a 2-gon requires the neighboring faces to share more than one edge. The alternative, that faces share more than one edge in the absence of a 2-gon (like the grains in Figure 26), is extremely rare.

While degenerate grains occur as a natural consequence of grain growth, they are not very frequent. Figure 27 shows that degenerate grains with 2-gon faces constitute less than 0.5% of all grains throughout our simulation. The initial increase in the number of these grains is a consequence of the possibility of generating a 2-gon when a 3-gon participates in a topological transition. The fraction of such grains saturates because the action of capillary pressure causes 2-gons to quickly disappear, with the result depending on the grain type.

Most of the degenerate grains in the Evolved microstructure have exactly one 2-gon (97%), and the disappearance of the 2-gon makes these grains polytopal. The 0.6% of the degenerate grains that are the trihedron shown in Figure 25(a) disappear entirely following the disappearance of one of the 2-gons since the result has a forbidden topology. The 1.6% of the degenerate grains with two 2-gons and the remaining 0.6% (except for the trihedron) with three or more 2-gons generally undergo
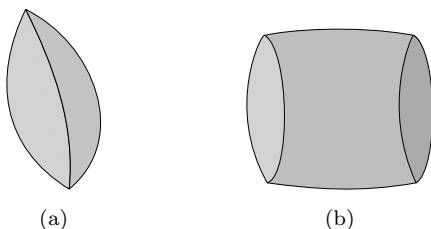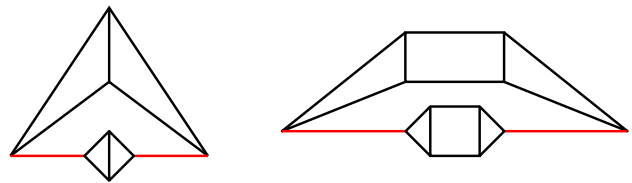

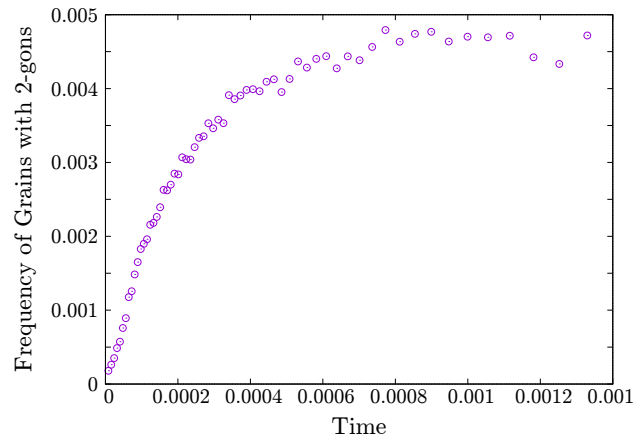FIG. 26. Examples of degenerate grains with two faces sharing multiple edges.

FIG. 27. Fraction of grains with a 2-gon face over time.

further transitions.

The distributions of the number of faces in Figure 16 imply the existence of flag* grains in the Poisson–Voronoi and Evolved microstructures with some maximum number of faces. For the Poisson–Voronoi microstructure, the unique largest flag* grain with 31 faces is shown in Figure 28 and has split type $1:4:26$. For the Evolved microstructure, the two largest grains with 38 faces are shown in Figure 29 and have split type $2:4:32$. These examples show that, as one might expect, grains with the maximum number of faces generally have little combinatorial constriction.

The grains with the most combinatorial constriction (in the sense of the penalty function) generally have severe geometrical constriction as well. The example from the Poisson–Voronoi microstructure in Figure 30 is notably extended along the axis perpendicular to the 4-belt, and the example from the Evolved microstructure
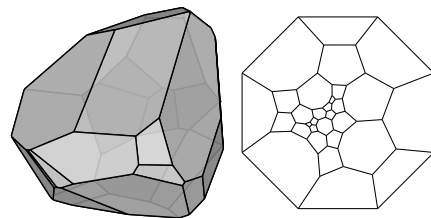

FIG. 25. Examples of degenerate grains with 2-gon faces. (a) The trihedron, and (b) the pillow.

FIG. 28. Extremal grain with 31 faces, type $1:4:26$, and p-vector $(0, 4, 13, 7, 5, 2)$ from the Poisson–Voronoi microstructure.
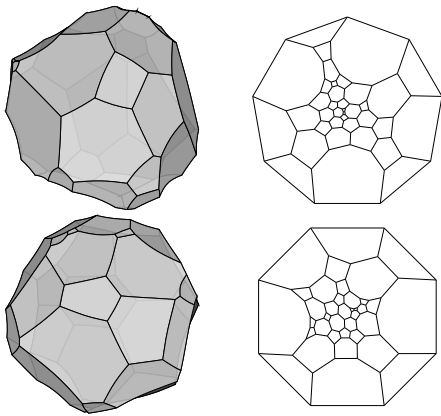
FIG. 29. Extremal grains with 38 faces, type $2:4:32$, and p-vectors $(0, 9, 8, 12, 5, 3, 1)$ and $(0, 10, 8, 8, 8, 4)$ from the Evolved microstructure.
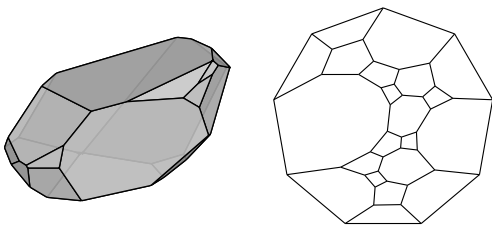

FIG. 30. Extremal grain with 22 faces, type $9:4:9$, and p-vector $(0, 7, 7, 3, 3, 0, 2)$ from the Poisson–Voronoi microstructure.

in Figure 31 visibly curves in along the 4-belt.

V. CONCLUSION

The grain growth microstructure is an unusual physical system in the sense that the governing equation is relatively simple, and yet reasonable explanations for quantities as basic as the average number of faces continue to elude researchers. Our main purpose here is not to resolve this situation, but rather to use the grain growth microstructure as motivation to develop novel topological and combinatorial concepts.

Grain growth dynamics strongly encourages the collapse of triangles once they are formed. This suggests classifying simple 3-polytopes as *fundamental* polytopes
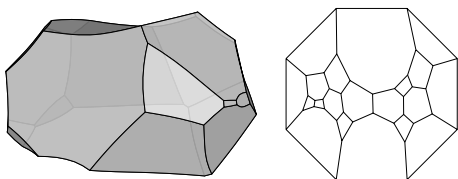

FIG. 31. Extremal grain with 21 faces, type $8:4:9$, and p-vector $(0, 6, 6, 5, 2, 2)$ from the Evolved microstructure.

without triangular faces (except for the tetrahedron), or *vertex-truncated* polytopes with triangular faces. Vertex-truncated polytopes are less stable with respect to topological transitions, and every vertex-truncated polytope can be reduced to a unique fundamental polytope by reversing vertex truncations.

The fundamental simple 3-polytopes therefore provide a useful point to begin investigating the combinatorial types of polytopes in the grain growth microstructure. Not all fundamental polytopes are equally frequent, though. Those that have a non-trivial belt of three faces passing around the polytope are said to be *severely constricted*, and appear only infrequently in the grain growth microstructure. The remaining fundamental polytopes (except for the tetrahedron) are said to be *flag**.

That the examples of severely constricted polytopes in our simulated microstructure are all severely geometrically constricted as well suggests that grain growth dynamics favors grains that are round — both geometrically and combinatorially. More specifically, a simple 3-polytope is *combinatorially k-round* if it is at most k truncations away from a non-severely constricted fundamental polytope. Our simulations provide extensive evidence that k-round grains for small values of k appear vastly more often in space-filling microstructures than could be expected from the distribution of the combinatorial types of all simple 3-polytopes. Moreover, the combinatorial roundness is positively correlated with the geometric roundness (as expressed by the isoperimetric quotient) for all three simulated microstructures considered here. That is, the definition of combinatorial roundness proposed in Section II B seems to be natural in the sense of capturing a meaningful and non-trivial aspect of the physical system.

Although the combinatorial roundness of a simple 3-polytope is related to the frequency of that polytope in a generic microstructure, this relationship is not precise. In fact, the examples of the Kelvin foam and the Weaire–Phelan foam show that the frequency of a polytope cannot, in general, be a function of combinatorial information alone. Instead, a penalty function is proposed, where the penalty increases with the number of faces and with the constriction as quantified by belts of faces around the polytope. This is intended to assign a value to the difficulty of accommodating the polytope in a space-filling microstructure, and (per Figure 21) seems to function as an upper bound for the frequency of the polytope.

Having developed this mathematical machinery, a particular microstructure derived from the Poisson–Voronoi initial condition is identified as containing an unusually large proportion of round grains. This Round microstructure has an average of 14.036 faces per grain (suggestively close to the 14 faces per grain of the Kelvin foam), and is conjectured to be more resistant to topological change than the steady-state grain growth microstructure. The investigation of the mechanical properties of the Round microstructure is proposed as a subject for further research.

ACKNOWLEDGMENTS

Appendix A: Combinatorial Constraints

The *face vector* of a 3-dimensional polytope is the triple $f = (f_0, f_1, f_2)$ of the numbers of vertices, edges, and faces of the polytope, respectively. A simple 3-polytope P with n faces, e edges, and t vertices has the face vector $f_P = (t, e, n)$, while the dual simplicial 3-polytope P^* has the face vector $f_{P^*} = (n, e, t)$. The Euler characteristic of P^* requires that $n - e + t = 2$, and equating the number of edge-triangle incidences and the number of triangle-edge incidences of P^* gives $2e = 3t$. Taken together, these imply that $f_{P^*} = (n, 3n-6, 2n-4)$, and by duality, that $f_P = (2n - 4, 3n - 6, n)$.

For any vertex v_i of P^*, the *degree* $\deg(v_i)$ of the vertex is the number of adjoining edges. Equating the number of vertex-edge incidences and the number of edge-vertex incidences of P^* gives $\sum_{i=1,\ldots,n} \deg(v_i) = 2e = 6n - 12$. The average vertex-degree of P^* is then

$$\overline{\deg} = \frac{1}{n} \sum_{i=1,\ldots,n} \deg(v_i) = 6 - \frac{12}{n} < 6. \tag{A1}$$

One of the implications of Equation A1 is that every simplicial 3-polytope has at least one vertex v with degree $\deg(v) < 6$. A second implication comes from the observation that since the degree of every vertex of a flag simplicial 3-polytope is at least 4, the average vertex-degree must be at least 4 as well. Equation A1 then requires that $n \geq 6$ for all flag simplicial 3-polytopes. The octahedron is the unique example with $n = 6$ vertices.

The *p-vector* of a 3-dimensional polytope is the tuple $p = (p_3, p_4, p_5, \ldots, p_{\max})$ of the numbers of 3-gons (triangles), 4-gons, 5-gons, etc. of the polytope, with $p_{\max}$ being the number of polygons with the maximum number of sides. Eberhard's theorem [23] states that for every sequence $\hat{p} = (p_3, p_4, p_5; p_7, p_8, \ldots, p_{\max})$ of nonnegative integers satisfying

$$3p_3 + 2p_4 + p_5 = 12 + \sum_{7 \leq k \leq \max} (k - 6)p_k \tag{A2}$$

and some nonnegative integer $p_6 \geq 0$, there is a simple 3-polytope with p-vector $p = (p_3, p_4, p_5, p_6, p_7, \ldots, p_{\max})$. The allowed values of p_6 are known in several cases. For example, the partial p-vector $(0, 0, 12)$ allows simple 3-polytopes for all $p_6 \neq 1$ [20, p. 271]; cf. also [24]. However, there is no 13-faced simple 3-polytope with $p = (0, 0, 12, 1)$.

Three-dimensional grain growth simulations generally use periodic boundary conditions, and represent the microstructure as a simple decomposition of the 3-dimensional torus T^3 into simple 3-polytopes. Let the dual triangulation T of any simple decomposition of T^3 have face vector $f_T = (f_0, f_1, f_2, f_3)$. The Euler characteristic of T requires that $f_0 - f_1 + f_2 - f_3 = 0$, and equating the number of triangle-tetrahedra incidences and the number of tetrahedra-triangle incidences gives $2f_2 = 4f_3$. These imply that $f_T = (f_0, f_1, 2f_1 - 2f_0, f_1 - f_0)$, or that the face vector is completely determined by f_0 and f_1.

The number of edges of any triangulation of a closed 3-manifold M is bounded above by the number of distinct pairs of vertices of the triangulation, or $f_1 \leq \binom{f_0}{2}$. A triangulation of M is called *neighborly* if f_1 achieves this bound. According to Walkup [25], there is a largest integer $\gamma(M)$ such that for every triangulation of M with f_0 vertices and f_1 edges the following inequality is satisfied:

$$f_1 \geq 4f_0 + \gamma(M). \tag{A3}$$

Moreover, for any 3-manifold M there is a smallest integer $\gamma^*(M) \geq \gamma(M)$ such that there is a triangulation of M for every pair of integers (f_0, f_1) provided that $f_0 \geq 0$ and that the following inequalities are satisfied:

$$\binom{f_0}{2} \geq f_1 \geq 4f_0 + \gamma^*(M). \tag{A4}$$

Specifically for the 3-torus T^3, the best known upper bounds are $\gamma^*(T^3) \leq 45$ and $\gamma(T^3) \leq 44$, and the best known lower bounds are $\gamma^*(M) \geq \gamma(M) \geq 11$ [26]. Equation A4 then implies that there are neighborly triangulations of T^3 for any $f_0 \geq 15$.

Analogously to a single simplicial 3-polytope, the average vertex-degree of a triangulation of the 3-dimensional torus T^3 is

$$\overline{\deg} = \frac{1}{f_0} \sum_{i=1,\ldots,n} \deg(v_i) = \frac{2f_1}{f_0}. \tag{A5}$$

This implies that when $f_1 = 4f_0 + \gamma(T^3)$ as in Equation A3, the average degree is $8 + 2\gamma(T^3)/f_0$, and that the average degree of a neighborly triangulation is $f_0 - 1$. Since there is no upper bound on f_0, the average degree satisfies $8 < \overline{\deg} < \infty$. That is, there are simple decompositions of T^3 into grains with the combinatorial types of simple 3-polytopes where the average number of faces per grain is as few as 8 or as many as the number of 3-polytopes in the decomposition minus one.

The arguments above do not require all grains to be proper convex 3-polytopes (not just combinatorial types)
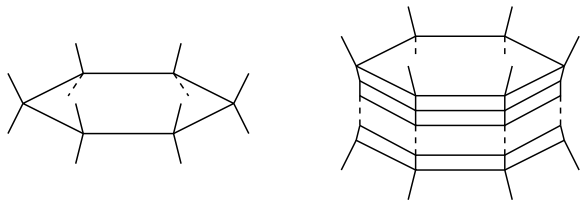
FIG. 32. A 6-gon in a simple cellular microstructure (left) and its expansion into prisms over the 6-gon (right).

FIG. 33. The star (in grey) and the link (in bold) of a vertex.

with planar faces and straight edges, though. Let this condition be called *geometric*. Poisson–Voronoi decompositions have an average of $48\pi^2/35 + 2 \simeq 15.535$ faces per grain [16], and are clearly geometric. The lower bound on the average number of faces can be achieved by replacing some of the vertices of any initial geometric decomposition with (small) tetrahedra. Repeating this procedure produces a geometric decomposition with an average number of faces per grain arbitrarily close to 8. The upper bound can be achieved by observing that a q-gon in a geometric decomposition can always be expanded into a prism over the q-gon. Repeating this procedure produces a geometric simple decomposition with an average number of faces per grain arbitrarily close to $2q + 2$; see Figure 32 for this construction over the 6-gon. Since there is some geometric decomposition that contains a q-gon for any choice of q, the average number of faces per grain of a geometric decomposition can be arbitrary large (we are grateful to John M. Sullivan for pointing this out). Note that this construction is dual to applying a sequence of stellar subdivisions to an edge of degree q as described by Luo and Stong [27].

Lemma 13 *There are geometric simple decompositions with average number of faces per grain ranging over*

$$8 < \frac{2f_1}{f_0} < \infty, \qquad (A6)$$

where f_0 and f_1 are the numbers of grains and of faces (corresponding to f_0 vertices and f_1 edges of the dual triangulations), respectively.

The lemma notwithstanding, examples of generic random decompositions with an average number of faces per grain substantially higher than that of the Poisson–Voronoi case (15.535) are not known.

Several analytical models predict the average number of faces per grain for particular simple decompositions. Coxeter [28] gives a value of 13.564, whereas Kusner [19, 29, 30] proved a lower bound of 13.397 on the average number of faces for a cell in an equal volume equal pressure foam. It would be of strong interest to provide further insight into the reasons why simple material microstructures seem to be narrowly confined to an average of between 12 and 16 faces per grain though, the more so since topology and geometry alone do not seem to enforce any restrictions.
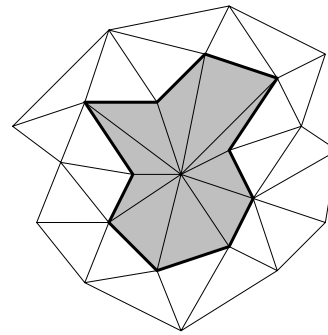
Appendix B: Algorithmic Aspects

The following is a brief sketch on how to algorithmically determine combinatorial information (stacked, flag, severely constricted, split type) for a given triangulation T of the 2-dimensional sphere S^2.

Let T have n vertices. If T has at least one vertex of degree 3, then T is either the boundary of the tetrahedron, in which case the combinatorial type of T is fully determined, or T has at least 5 vertices.

Definition 14 *The* star *of a vertex v in a triangulation T of S^2 is written as $\mathrm{star}_v T$, and is the collection of faces of T that contain the vertex v and all of their subfaces (shown in Figure 33). The* link *of v in T is written as $\mathrm{link}_v T$, and is the collection of all faces in $\mathrm{star}_v T$ that do not contain v.*

If $\mathrm{star}_v T$ consists of m triangles (and their subfaces), then $\mathrm{link}_v T$ is a cycle of length m. In particular, if v is a vertex of degree 3, then $\mathrm{link}_v T$ is a cycle with three vertices a, b and c, and edges ab, ac, and bc. If the three triangles abv, acv, and bcv of $\mathrm{star}_v T$ are removed and replaced by the single triangle abc, then this is a local modification that undoes a stacking operation, and yields a triangulation of S^2 with $n - 1$ vertices.

Given the triangulation T, we iteratively remove vertices of degree 3 (in any order) until the result is either

- the boundary of the tetrahedron
- or a triangulation with no vertex of degree 3 (flag or severely constricted).

If this process results in the boundary of the tetrahedron, then T is a stacked triangulation that is $n - 4$ stackings away from the boundary of the tetrahedron. If a triangulation T' without vertices of degree 3 is reached, we search for empty traingles to identify whether the resulting triangulation is flag or severely constricted. To do so, for every set of three vertices e, f and g of T', we check whether ef, eg and fg are edges of T'. If they are, we check whether or not efg is a triangle of the triangulation T'. If it is not, then efg is an empty triangle, and T' is severely constricted. If T' has no empty triangle, then it is flag.

To determine the split type of a flag triangulation T with n vertices, we generate all cycles of length four in the 1-skeleton of T. To do so, we consider all subsets of four vertices a, b, c, and d of the vertices of T. For each subset, we check if one of the cycles a–b–c–d–a, a–b–d–c–a, or a–c–b–d–a is contained in the 1-skeleton of T. For every 4-cycle in the 1-skeleton of T, we compute the split of T with respect to this 4-cycle.

The split of the 4-cycle a–b–c–d–a in the 1-skeleton of T is found by splitting $\mathrm{star}_a T$ into two parts along a–b–c–d–a. The two parts can be extended by a greedy search into the two components of the overall split. Finally, the numbers of vertices on each side are found (excluding the four vertices a, b, c and d on the splitting cycle). The largest $k \leq \frac{n-4}{2}$ for which there is a split $k\!:\!4\!:\!(n-4-k)$ determines the split type of T.

[1] J. E. Burke and D. Turnbull, Progr. Metal Phys. **3**, 220 (1952).
[2] C. S. Smith, in *Metal Interfaces* (ASM: Cleveland, OH, 1952) pp. 65–113.
[3] E. A. Lazar, J. K. Mason, R. D. MacPherson, and D. J. Srolovitz, Acta Materialia **59**, 6837 (2011).
[4] J. K. Mason, E. A. Lazar, R. D. MacPherson, and D. J. Srolovitz, Phys. Review E **92**, 063308 (2015).
[5] E. A. Lazar, J. K. Mason, R. D. MacPherson, and D. J. Srolovitz, Phys. Rev. Lett. **109**, 095505 (2012).
[6] D. L. Weaire and S. Hutzler, *The Physics of Foams* (Oxford University Press, 2001).
[7] V. Schlegel, Nova Acta Acad. Leop.-Carol. **44** (1881).
[8] V. Schlegel, "Projections-Modelle der sechs regelmässigen vier-dimensionalen Körper und des vier-dimensionalen vierseitigen Prismas," (1886).
[9] K. Brown, *Buildings* (Springer, 1989).
[10] D. Kozlov, *Combinatorial Algebraic Topology*, Algorithms and Computation in Mathematics, Vol. 21 (Springer, 2007).
[11] C. A. Athanasiadis, Ark. Mat. **49**, 17 (2011).
[12] F. Rhines and B. Patterson, Metallurgical Trans. A **13**, 985 (1982).
[13] B. R. Patterson, D. J. Rule, R. DeHoff, and V. Tikare, Acta Materialia **61**, 3986 (2013).
[14] G. Brinkmann and B. McKay, "`plantri`: a program for generating planar triangulations and planar cubic graphs," `http://cs.anu.edu.au/people/bdm/plantri/` (1996–2001), version 4.1.
[15] F. H. Lutz, "The Manifold Page, 1999–2017," `http://page.math.tu-berlin.de/~lutz/stellar/`.
[16] J. L. Meijering, Philips Research Reports **8**, 270 (1953).
[17] W. S. Thomson, Acta Math. **11**, 121 (1887).
[18] D. Weaire and R. Phelan, Philosophical Magazine Letters **69**, 107 (1994).
[19] R. Kusner and J. M. Sullivan, Forma **11**, 233 (1996).
[20] B. Grünbaum, *Convex Polytopes*, Pure and Applied Mathematics, Vol. 16 (Interscience Publishers, London, 1967) second edition (V. Kaibel, V. Klee, and G. M. Ziegler, eds.), Graduate Texts in Mathematics **221**. Springer-Verlag, New York, NY, 2003.
[21] J. M. Sullivan, in *Foams, Emulsions and Their Applications,* Proc. 3rd EuroConference on Foams, Emulsions and Applications (EuroFoam 2000), Delft, the Netherlands, 2000, edited by P. L. J. Zitha, J. Banhart, and G. Verbist (Verlag MIT Publishing, Bremen, 2000) pp. 111–119.
[22] F. H. Lutz, in *Discrete Differential Geometry*, Oberwolfach Seminars, Vol. 38, edited by A. I. Bobenko, P. Schröder, J. M. Sullivan, and G. M. Ziegler (Birkhäuser, Basel, 2008) pp. 235–253.
[23] V. Eberhard, *Zur Morphologie der Polyeder* (B. G. Teubner, Leipzig, 1891).
[24] I. Izmestiev, R. B. Kusner, G. Rote, B. Springborn, and J. M. Sullivan, Geometriae Dedicata **166**, 15 (2013).
[25] D. W. Walkup, Acta Math. **125**, 75 (1970).
[26] F. H. Lutz, T. Sulanke, and E. Swartz, Electron. J. Comb. **16**, No. 2, Research Paper R13, 33 p. (2009).
[27] F. Luo and R. Stong, Trans. Am. Math. Soc. **337**, 891 (1993).
[28] H. S. M. Coxeter, Illinois Journal of Mathematics **2**, 746 (1958).
[29] N. Rivier and A. Lissowski, J. Physics A: Math. Gen. **15**, L143 (1982).
[30] R. Kusner, Proc. Royal Soc. London, Series A, Math. and Phys. Sciences **439**, 683 (1992).

TABLE II. The number of all possible triangulations of the 2-sphere for small numbers of vertices n [14]. The degree of a vertex is the number of adjoining edges.

n	all	min. deg. ≥ 4	flag
4	1	0	0
5	1	0	0
6	2	1	1
7	5	1	1
8	14	2	2
9	50	5	4
10	233	12	10
11	1249	34	25
12	7595	130	87
13	49566	525	313
14	339722	2472	1357
15	2406841	12400	6244
16	17490241	65619	30926
17	129664753	357504	158428
18	977526957	1992985	836749
19	7475907149	11284042	4504607
20	57896349553	64719885	24649284
21	453382272049	375126827	136610879
22	3585853662949	2194439398	765598927
23	28615703421545	12941995397	4332047595
24		76890024027	24724362117
25		459873914230	142205424580
26		2767364341936	823687567019
27		16747182732792	4801749063379

TABLE III. The number of triangulations of the 2-sphere that belong to the classes defined in Section II B for small numbers of vertices n.

n	all	stacked	flag	flag$_{+1}$	flag$_{+1+1}$	flag$_{+2}$	flag$_{\geq 3}$	sc*	sc$^*_{+1}$	sc$^*_{>2}$
4	1	1	0	0	0	0	0	0	0	0
5	1	1	0	0	0	0	0	0	0	0
6	2	1	1	0	0	0	0	0	0	0
7	5	3	1	1	0	0	0	0	0	0
8	14	7	2	1	3	1	0	0	0	0
9	50	24	4	3	5	2	11	1	0	0
10	233	93	10	13	19	7	86	2	3	0
11	1249	434	25	47	78	30	590	9	16	20
12	7595	2110	87	217	354	127	4301	43	99	257
13	49566	11002	313	1041	1799	608	30938	212	650	3003
14	339722	58713	1357	5288	9780	3016	224839	1115	3997	31617

TABLE IV. The number of simple 3-polytopes in `V-268402` that belong to the various classes defined in Section II B, where n is the number of faces. The final row is the sum of entries in the column.

n	all	stacked*	flag*	flag$^*_{+1}$	flag$^*_{+1+1}$	flag$^*_{+2}$	flag$^*_{\geq 3}$	sc	sc$_{+1}$	sc$_{\geq 2}$
4	0	0	0	0	0	0	0	0	0	0
5	14	14	0	0	0	0	0	0	0	0
6	94	71	23	0	0	0	0	0	0	0
7	451	188	99	164	0	0	0	0	0	0
8	1556	348	311	453	312	132	0	0	0	0
9	4063	385	812	1177	697	188	788	16	0	0
10	8208	389	1371	2350	1661	327	2027	29	54	0
11	14012	252	2219	3723	3001	569	4058	39	76	75
12	20650	152	3037	5408	4516	659	6580	43	89	166
13	26615	64	3351	6899	5983	759	9153	45	103	258
14	30987	30	3589	7568	7252	792	11263	45	117	331
15	32304	8	3338	7456	7615	791	12663	38	76	319
16	30721	1	2772	6636	7402	640	12908	11	69	282
17	27189	0	2366	5363	6297	560	12271	12	60	260
18	22195	0	1648	4317	5268	389	10345	14	37	177
19	17018	0	1112	3145	3906	302	8398	6	27	122
20	12090	0	742	2103	2680	157	6281	9	15	103
21	8139	0	456	1317	1768	110	4429	4	9	46
22	5182	0	266	772	1059	72	2970	3	7	33
23	3090	0	157	431	628	37	1821	1	3	12
24	1794	0	69	219	355	19	1125	0	0	7
25	998	0	40	117	192	13	629	0	0	7
26	542	0	10	57	92	7	373	0	0	3
27	265	0	12	18	40	4	187	0	0	4
28	120	0	8	10	19	2	80	0	1	0
29	63	0	1	7	11	0	44	0	0	0
30	28	0	0	3	5	0	20	0	0	0
31	9	0	1	1	0	1	6	0	0	0
32	2	0	0	1	0	0	1	0	0	0
33	2	0	0	0	0	0	2	0	0	0
34	1	0	0	0	1	0	0	0	0	0
	268402	1902	27810	59715	60760	6530	108422	315	743	2205

TABLE V. The number of simple 3-polytopes in `R-268402` that belong to the various classes defined in Section II B, where n is the number of faces. The final row is the sum of entries in the column.

n	all	stacked*	flag*	flag$^*_{+1}$	flag$^*_{+1+1}$	flag$^*_{+2}$	flag$^*_{>3}$	sc	sc$_{+1}$	sc$_{\geq 2}$
4	124	124	0	0	0	0	0	0	0	0
5	676	676	0	0	0	0	0	0	0	0
6	1998	899	1099	0	0	0	0	0	0	0
7	4054	548	2021	1485	0	0	0	0	0	0
8	7699	203	4965	1680	514	337	0	0	0	0
9	12383	45	8607	2721	549	119	290	52	0	0
10	17610	9	12579	3752	712	199	286	52	21	0
11	22876	3	16698	4742	956	138	265	42	20	12
12	26736	1	19758	5454	1062	150	253	40	16	2
13	29072	0	21249	6164	1209	145	273	19	8	5
14	29201	0	21211	6326	1237	101	288	20	6	12
15	27267	0	19613	6074	1222	91	244	13	7	3
16	23688	0	16942	5335	1103	55	241	7	4	1
17	19618	0	13824	4543	990	56	200	4	1	0
18	15154	0	10463	3637	794	44	208	3	4	1
19	10882	0	7372	2732	606	24	143	3	2	0
20	7649	0	5215	1836	481	20	97	0	0	0
21	4921	0	3295	1232	308	9	76	1	0	0
22	2977	0	1929	804	190	8	46	0	0	0
23	1780	0	1154	442	135	3	46	0	0	0
24	1016	0	633	262	97	1	23	0	0	0
25	539	0	344	134	39	3	19	0	0	0
26	268	0	165	74	24	0	5	0	0	0
27	122	0	78	35	5	0	4	0	0	0
28	54	0	37	12	3	0	2	0	0	0
29	23	0	14	7	2	0	0	0	0	0
30	4	0	4	0	0	0	0	0	0	0
31	10	0	8	2	0	0	0	0	0	0
32	1	0	1	0	0	0	0	0	0	0
	268402	2508	189278	59485	12238	1503	3009	256	89	36

TABLE VI. The number of simple 3-polytopes in `E-268402` that belong to the various classes defined in Section II B, where n is the number of faces. The final row is the sum of entries in the column.

n	all	stacked*	flag*	flag*$_{+1}$	flag*$_{1+1}$	flag*$_{+2}$	flag*$_{>3}$	sc	sc$_{+1}$	sc$_{\geq 2}$
4	372	372	0	0	0	0	0	0	0	0
5	1840	1840	0	0	0	0	0	0	0	0
6	4850	2521	2329	0	0	0	0	0	0	0
7	9362	1629	4001	3732	0	0	0	0	0	0
8	14627	674	8122	3656	1364	811	0	0	0	0
9	19097	163	11489	4891	1207	414	804	129	0	0
10	22550	30	14264	5498	1514	352	716	96	80	0
11	23512	3	15138	5781	1577	248	610	80	45	30
12	24041	1	15495	6111	1568	209	557	35	43	22
13	22445	1	14302	5902	1546	122	505	24	21	22
14	21241	0	13478	5621	1436	125	544	16	12	9
15	18712	0	11507	5151	1431	103	501	7	9	3
16	16585	0	9927	4700	1429	80	426	7	11	5
17	14215	0	8295	4135	1298	69	407	5	3	3
18	11997	0	6691	3667	1144	55	431	1	5	3
19	9898	0	5342	3156	1006	46	345	0	3	0
20	7958	0	4153	2559	877	33	334	2	0	0
21	6438	0	3223	2076	794	17	324	2	1	1
22	5077	0	2459	1695	637	25	257	1	0	3
23	3755	0	1686	1256	568	13	231	0	1	0
24	2925	0	1318	973	431	12	191	0	0	0
25	2136	0	885	726	363	3	159	0	0	0
26	1480	0	571	547	229	9	123	0	1	0
27	1068	0	382	376	210	3	97	0	0	0
28	749	0	263	268	140	2	76	0	0	0
29	547	0	193	204	89	2	59	0	0	0
30	332	0	103	115	65	0	49	0	0	0
31	224	0	72	85	40	0	27	0	0	0
32	149	0	49	39	35	0	26	0	0	0
33	101	0	30	29	21	1	20	0	0	0
34	53	0	18	11	13	0	11	0	0	0
35	26	0	8	10	6	0	2	0	0	0
36	17	0	3	4	7	0	3	0	0	0
37	11	0	3	6	1	0	1	0	0	0
38	9	0	2	2	4	0	1	0	0	0
39	1	0	0	0	0	0	1	0	0	0
40	0	0	0	0	0	0	0	0	0	0
41	1	0	0	1	0	0	0	0	0	0
42	0	0	0	0	0	0	0	0	0	0
43	0	0	0	0	0	0	0	0	0	0
44	0	0	0	0	0	0	0	0	0	0
45	1	0	0	0	0	0	1	0	0	0
	268402	7234	155801	72983	21050	2754	7839	405	235	101

TABLE VII. Percentages of k-round grains for the V-268402, E-268402 and R-268402 data sets, and percentages of k-round grains for the same three data sets and for all simple 3-polytopes with $n = 13$ and $n = 14$.

	round$_0$	round$_{\leq 1}$	round$_{\leq 2}$	round$_{\leq 3}$	round$_{\leq 4}$	round$_{\leq 5}$	round$_{\leq 6}$	sc$_{\geq}$
V-268402	10.36	32.61	57.71	77.17	88.85	94.75	97.32	1.22
E-268402	58.19	86.06	95.87	98.79	99.54	99.69	99.72	0.28
R-268402	70.57	92.98	98.44	99.58	99.81	99.85	99.86	0.14
all$^*_{n=13}$	0.63	2.73	7.59	15.19	25.63	37.82	51.59	7.80
V-268402$_{n=13}$	12.59	38.51	63.84	81.81	91.21	95.65	97.41	1.53
E-268402$_{n=13}$	63.72	90.02	97.45	99.14	99.58	99.68	99.69	0.30
R-268402$_{n=13}$	73.09	94.29	98.95	99.76	99.86	99.89	99.89	0.11
all$^*_{n=14}$	0.40	1.96	5.72	12.04	20.81	31.36	43.11	10.81
V-268402$_{n=14}$	11.58	36.01	61.96	80.29	90.58	95.40	97.30	1.59
E-268402$_{n=14}$	63.45	89.92	97.26	99.32	99.73	99.81	99.82	0.17
R-268402$_{n=14}$	72.64	94.30	98.88	99.72	99.85	99.87	99.87	0.13

TABLE VIII. Number of flag triangulations of the 2-sphere with n vertices and split type $k{:}m$.

k n	0	1	2	3	4	5
6		1×1:1				
7		1×1:2				
8			2×2:2			
9		1×1:4	3×2:3			
10		2×1:5	1×2:4	7×3:3		
11		3×1:6	6×2:5	16×3:4		
12	1×0:8	9×1:7	15×2:6	16×3:5	46×4:4	
13		28×1:8	52×2:7	62×3:6	171×4:5	
14	1×0:10	97×1:9	209×2:8	235×3:7	261×4:6	554×5:5

TABLE IX. Number of flag* grains in `V-268402` with n faces and split type $k\!:\!m$.

n \ k	0	1	2	3	4	5	6	7	8	9
6		23×1:1								
7		99×1:2								
8			311×2:2							
9		172×1:4	640×2:3							
10		264×1:5	407×2:4	700×3:3						
11		536×1:6	711×2:5	972×3:4						
12	6×0:8	748×1:7	932×2:6	638×3:5	713×4:4					
13		903×1:8	1134×2:7	642×3:6	672×4:5					
14	1×0:10	1060×1:9	1166×2:8	648×3:7	426×4:6	288×5:5				
15	1×0:11	969×1:10	1167×2:9	609×3:8	300×4:7	292×5:6				
16	1×0:12	814×1:11	1005×2:10	472×3:9	220×4:8	153×5:7	107×6:6			
17	1×0:13	688×1:12	923×2:11	384×3:10	186×4:9	103×5:8	81×6:7			
18		534×1:13	647×2:12	269×3:11	100×4:10	48×5:9	29×6:8	21×7:7		
19		331×1:14	469×2:13	188×3:12	64×4:11	28×5:10	21×6:9	11×7:8		
20		234×1:15	334×2:14	108×3:13	38×4:12	10×5:11	13×6:10	4×7:9	1×8:8	
21		144×1:16	200×2:15	66×3:14	29×4:13	8×5:12	4×6:11	3×7:10	2×8:9	
22		82×1:17	113×2:16	49×3:15	15×4:14	5×5:13			1×8:10	1×9:9
23		63×1:18	54×2:17	31×3:16	6×4:15	2×5:14	1×6:13			
24		21×1:19	37×2:18	6×3:17	4×4:16				1×8:12	
25		14×1:20	19×2:19	3×3:18	4×4:17					
26		5×1:21	5×2:20							
27		1×1:22	9×2:21	1×3:20	1×4:19					
28		1×1:23	5×2:22	1×3:21	1×4:20					
29			1×2:23							
30										
31		1×1:26								

TABLE X. Number of fllag* grains in `R-268402` with n faces and split type $k{:}m$.

n \ k	0	1	2	3	4	5	6	7	8
6		1099×1:1							
7		2021×1:2							
8			4965×2:2						
9		3632×1:4	4975×2:3						
10		4895×1:5	3878×2:4	3806×3:3					
11		7676×1:6	4843×2:5	4179×3:4					
12	184×0:8	9577×1:7	5555×2:6	2617×3:5	1825×4:4				
13		11358×1:8	6030×2:7	2216×3:6	1645×4:5				
14	102×0:10	11957×1:9	5964×2:8	1816×3:7	867×4:6	505×5:5			
15	82×0:11	11673×1:10	5421×2:9	1390×3:8	626×4:7	421×5:6			
16	58×0:12	10511×1:11	4581×2:10	1099×3:9	387×4:8	195×5:7	111×6:6		
17	66×0:13	8793×1:12	3766×2:11	775×3:10	238×4:9	101×5:8	85×6:7		
18	38×0:14	6802×1:13	2846×2:12	541×3:11	141×4:10	57×5:9	20×6:8	18×7:7	
19	36×0:15	4930×1:14	1937×2:13	329×3:12	85×4:11	31×5:10	12×6:9	12×7:8	
20	16×0:16	3556×1:15	1353×2:14	206×3:13	58×4:12	17×5:11	5×6:10	2×7:9	2×8:8
21	12×0:17	2238×1:16	892×2:15	123×3:14	20×4:13	5×5:12	2×6:11	1×7:10	2×8:9
22	5×0:18	1324×1:17	500×2:16	77×3:15	18×4:14	5×5:13			
23	5×0:19	799×1:18	299×2:17	44×3:16	7×4:15				
24	1×0:20	462×1:19	152×2:18	17×3:17	1×4:16				
25	3×0:21	246×1:20	82×2:19	12×3:18	1×4:17				
26		127×1:21	37×2:20	1×3:19					
27	1×0:23	52×1:22	25×2:21						
28		22×1:23	14×2:22		1×4:20				
29		10×1:24	4×2:23						
30		4×1:25							
31		5×1:26	3×2:25						
32			1×2:26						

TABLE XI. Number of flag* grains in `E-268402` with n faces and split type $k{:}m$.

n \ k	0	1	2	3	4	5	6	7	8
6		2329×1:1							
7		4001×1:2							
8			8122×2:2						
9		5024×1:4	6465×2:3						
10		5941×1:5	4110×2:4	4213×3:3					
11		7347×1:6	4226×2:5	3565×3:4					
12	187×0:8	7739×1:7	4279×2:6	2001×3:5	1289×4:4				
13		7894×1:8	3993×2:7	1403×3:6	1012×4:5				
14	69×0:10	7855×1:9	3692×2:8	1091×3:7	493×4:6	278×5:5			
15	42×0:11	6964×1:10	3159×2:9	801×3:8	321×4:7	220×5:6			
16	38×0:12	6178×1:11	2742×2:10	626×3:9	200×4:8	98×5:7	45×6:6		
17	27×0:13	5278×1:12	2322×2:11	456×3:10	121×4:9	54×5:8	37×6:7		
18	28×0:14	4315×1:13	1858×2:12	349×3:11	92×4:10	28×5:9	13×6:8	8×7:7	
19	13×0:15	3513×1:14	1480×2:13	256×3:12	53×4:11	19×5:10	5×6:9	3×7:8	
20	19×0:16	2740×1:15	1155×2:14	179×3:13	40×4:12	11×5:11	6×6:10	3×7:9	
21	12×0:17	2127×1:16	911×2:15	144×3:14	18×4:13	8×5:12		1×7:10	2×8:9
22	5×0:18	1639×1:17	683×2:16	104×3:15	21×4:14	5×5:13	2×6:12		
23	1×0:19	1083×1:18	517×2:17	68×3:16	12×4:15	5×5:14			
24	3×0:20	851×1:19	401×2:18	56×3:17	6×4:16	1×5:15			
25	3×0:21	597×1:20	250×2:19	31×3:18	3×4:17		1×6:15		
26	1×0:22	382×1:21	169×2:20	16×3:19	3×4:18				
27	1×0:23	263×1:22	105×2:21	11×3:20	1×4:19	1×5:18			
28		168×1:23	84×2:22	11×3:21					
29		125×1:24	60×2:23	8×3:22					
30		75×1:25	24×2:24	4×3:23					
31		47×1:26	23×2:25	1×3:24		1×5:22			
32		35×1:27	13×2:26	1×3:25					
33		22×1:28	7×2:27	1×3:26					
34		10×1:29	7×2:28	1×3:27					
35		4×1:30	4×2:29						
36		2×1:31		1×3:29					
37		1×1:32	2×2:31						
38			2×2:32						